research report

Structural Design for Fire Conditions of a Prototype Metal Building using the New Proposed Appendix to AISI S100

RESEARCH REPORT RP22-02

May 2022

American Iron and Steel Institute

DISCLAIMER

The material contained herein has been developed by researchers based on their research findings and is for general information only. The information in it should not be used without first securing competent advice with respect to its suitability for any given application. The publication of the information is not intended as a representation or warranty on the part of the American Iron and Steel Institute or of any other person named herein, that the information is suitable for any general or particular use or of freedom from infringement of any patent or patents. Anyone making use of the information assumes all liability arising from such use.

COLD-FORMED STEEL RESEARCH CONSORTIUM

Final Technical Report

Project Title:

Structural Design for Fire Conditions of a Prototype Metal Building using the New Proposed Appendix to AISI S100

Prepared for the American Iron and Steel Institute (AISI) and
the Metal Building Manufacturers Association (MBMA)

Authors

Xia Yan
PhD Student
Department of Civil and Systems Engineering
Johns Hopkins University
Baltimore, MD

Thomas Gernay
Assistant Professor
Department of Civil and Systems Engineering
Johns Hopkins University
Baltimore, MD

Project start date: 1 July 2021
Project end date: 31 October 2021

(a) Acknowledgement of Support

This report is based upon work supported by the AISI Standards Council through the Small Fellowship Program. This support is gratefully acknowledged. The authors would also like to thank the industry advisors who provided consistently thoughtful advice, input, effort, and feedback throughout this project: Vincent Sagan from the Metal Building Manufacturers Association (MBMA), Andy Jaworski from Nucor Buildings Group, and Nestor Iwankiw from Jensen Hughes.

(b) Disclaimer

The views and conclusions contained in this document are those of the authors and should not be interpreted as representing the opinions of the American Iron and Steel Institute (AISI) or those of the Metal Building Manufacturers Association (MBMA). Mention of trade names of commercial products does not constitute their endorsement by AISI or MBMA.

Under a license agreement between Gesval S.A. and the Johns Hopkins University, Dr. Gernay and the University are entitled to royalty distributions related to the technology SAFIR described in the study discussed in this report. This arrangement has been reviewed and approved by the Johns Hopkins University in accordance with its conflict of interest policies.

Table of Contents

1. Introduction

Performance-based design for fire conditions has been increasingly adopted for different structural systems over the last decade. The objective of this project is to exemplify through a case study how the newly proposed Appendix 4 to AISI S100 [1] on 'Structural Design for Fire Conditions' could be used by the metal building industry. The scope of work on the project includes the following:

(1) Identification of a prototype metal building to serve as an exemplar case study for the structural fire design procedure.

(2) Definition of the performance objectives and design requirements for the building in the fire situation. This includes the determination of the applied loading based on load combinations relevant to the fire situation.

(3) Determination of a set of design-basis fires. The design-basis fires are based on the physical characteristics of the compartment, fuel, and ventilation conditions. The ASTM E119 [2] standard fire is also considered.

(4) Determination of the temperature distributions in the members of the building structure based on heat transfer analyses. Finite element thermal analyses of the section of the members are conducted taking into account the thermal exposures generated by the design-basis fires and the temperature-dependent thermal properties of the materials.

(5) Determination of the structural response and strength of the metal building structure in the fire situation. The Direct Strength Method (DSM) of the AISI S100 [1] design standard is used to calculate the capacity of the structure considering the reduction of mechanical properties due to temperature. Finite element analyses of the structure are also conducted, taking into account large displacements and effects of temperature, to compare the results of a numerical analysis method with those of the DSM.

(6) Verification that the design meets the performance objectives in the fire situation.

(7) Characterization of the fire rating of UL-assemblies using heat transfer analysis and the prescriptive limiting steel temperature criteria. This serves to compare the outcomes of the analysis method with the physical testing qualifications, as well as to analyze assemblies that are currently not rated by UL.

(8) Summary of the work and findings.

2. Scope and objectives

2.1. Prototype building

The prototype building in this study is a one-story warehouse located in Greeley, Colorado, as shown in Figure 1, designed in accordance with the 2018 International Building Code [3]. The floor plan is 75 ft x 120 ft. The eave height is 20 ft, and the roof has a symmetric gable roof configuration with 1:12 slope. The external walls are corrugated metal panels. About 10 % of the wall area are openings for windows and doors. An interior partition wall divides the building into a large warehouse and a small office area. The dimensions of the warehouse area are 75 ft x 108 ft, as shown in Figure 2.

Figure 1 Prototype warehouse building.

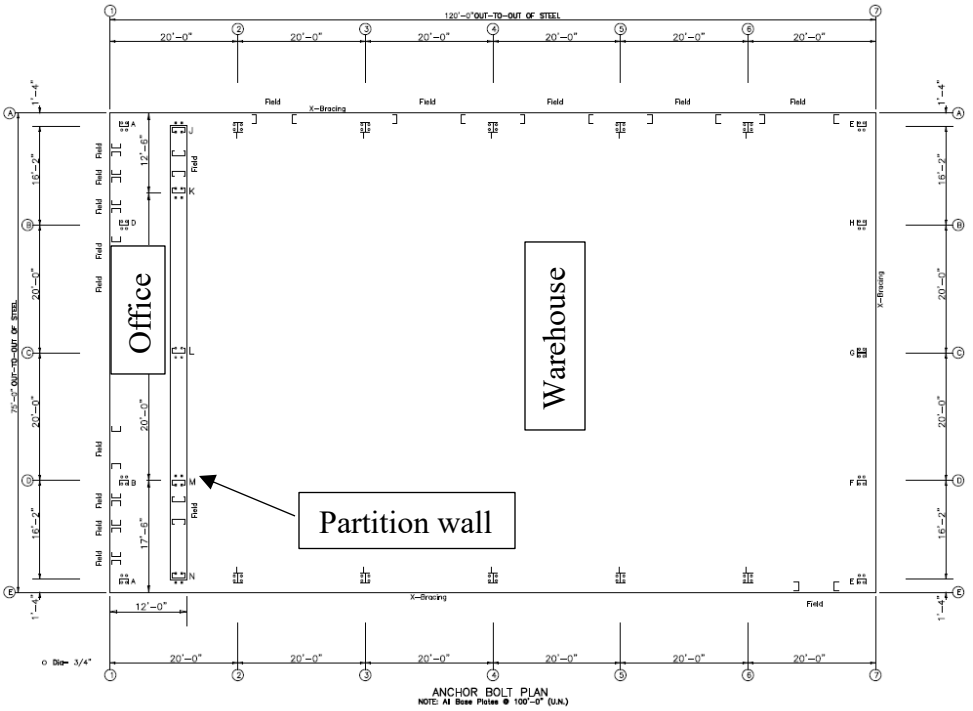

Figure 2 Floor plan of the warehouse.

2.2. End walls

The study focuses on the two end walls of the prototype building structure designed as Type IIB Construction and moderate-hazard storage, Use Group S-1, under the building code. The end walls are framed with cold-formed steel columns and beams, as shown in Figure 3 and Figure 4. The columns are composed of single and double C-shaped sections, as shown in Figure 5. Dimensions of the columns are listed in Table 1. Wall girts are placed at three elevations: 7.5 ft, 13.5 ft, and 17 ft, which also provides bracing to the columns. In-line attachments between girts and columns are used for the end wall framing line 1, i.e., the girts are in plane with the columns. Bypass girt attachments are used for the end wall framing line 7. The unbraced length for the major and minor axis bending of each column is given in Table 2. The columns of the end wall framing are fire-resistance-rated assemblies with Type X gypsum board for a 1-hour duration, which would be required by code if the building separation distance was less than 30 feet. The rafters do not require fire protection given the building's Type IIB Construction classification and the height of the roof.

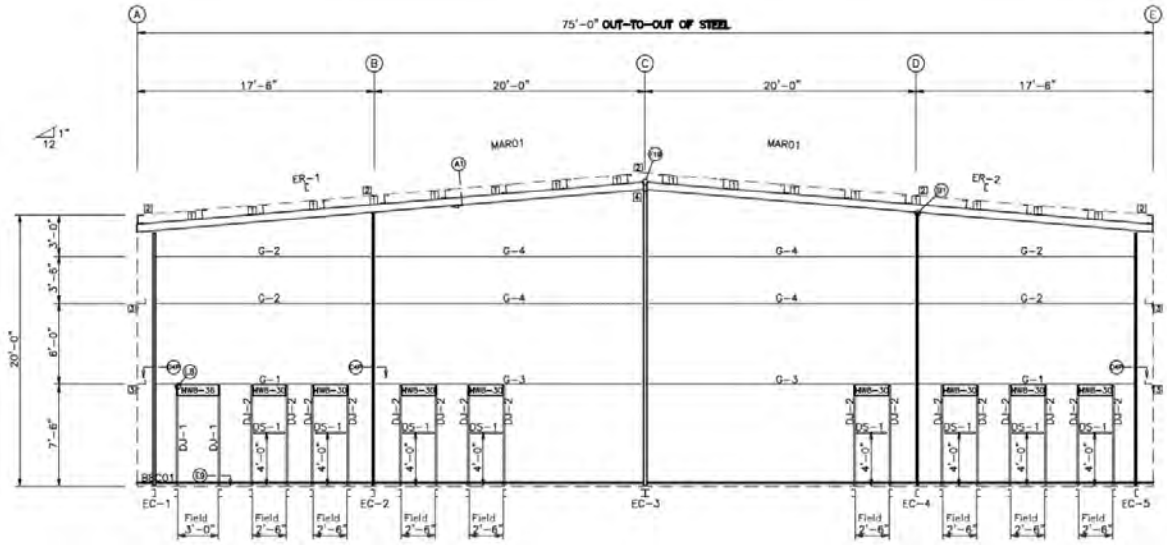

Figure 3 End wall framing line 1.

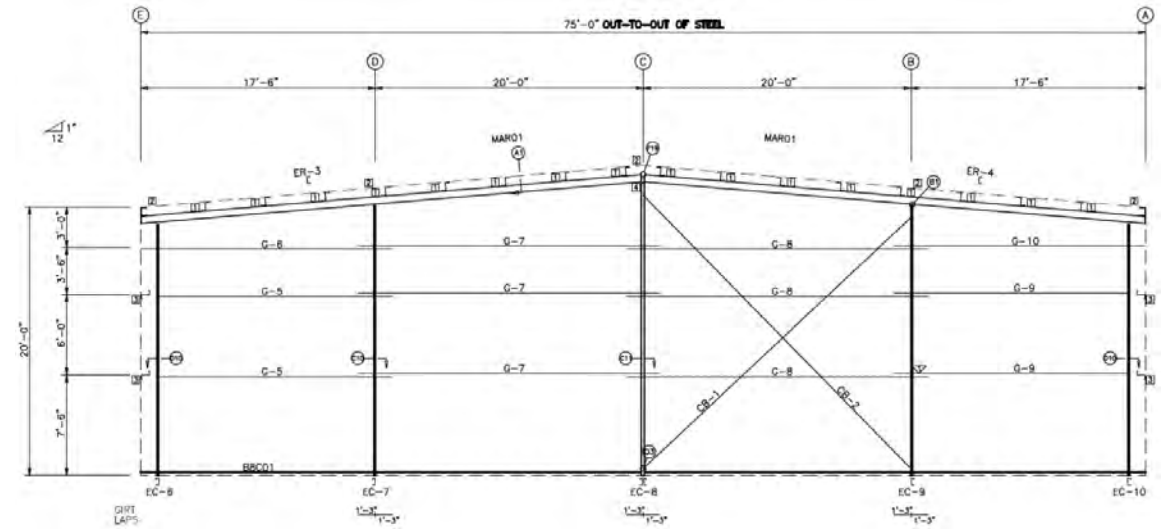

Figure 4 End wall framing line 7.

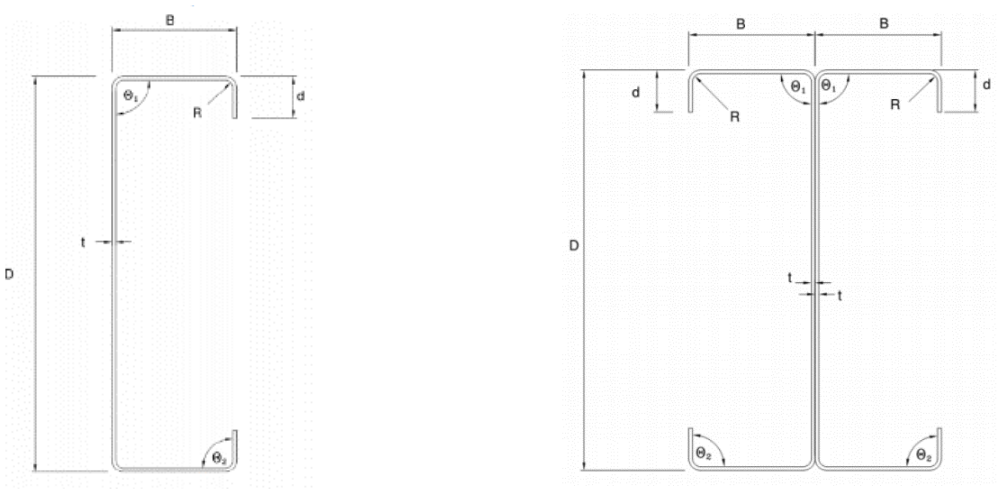

(1) Single C-shaped section (2) Double C-shaped section

Figure 5 C-shaped sections used for the columns of the end walls.

Table 1 Section dimensions of the end wall columns.

Location	Column	Grade (ksi)	Part	D (in.)	B (in.)	R (in.)	d (in.)	t (in.)
End wall framing line 1	EC-1	55	W08S075	8	3.78	0.25	0.992	0.075
	EC-2	55	W08S120	8	3.78	0.25	1.101	0.120
	EC-3	55	W08SD099	8	3.78	0.25	1.050	0.099
	EC-4	55	W12S099	12	3.63	0.25	1.049	0.099
	EC-5	55	W08S075	8	3.75	0.25	0.992	0.075
End wall framing line 7	EC-6	55	W08S075	8	3.78	0.25	0.992	0.075
	EC-7	55	W08S120	8	3.78	0.25	1.101	0.120
	EC-8	55	W08SD099	8	3.78	0.25	1.050	0.099
	EC-9	55	W12S099	12	3.63	0.25	1.049	0.099
	EC-10	55	W08S075	8	3.75	0.25	0.992	0.075

Table 2 Unbraced length of the columns.

Location	Column	Major axis (ft)	Minor axis (ft)
End wall framing line 1	EC-1	18.4	7.5
	EC-2	19.8	7.5
	EC-3	21.5	7.5
	EC-4	19.8	7.5
	EC-5	18.4	7.5
End wall framing line 7	EC-6	18.4	7.5
	EC-7	19.8	7.5
	EC-8	21.5	7.5
	EC-9	19.8	7.5
	EC-10	18.4	7.5

2.3. Performance objectives

The study focuses on the loadbearing stability of the fire-resistance-rated members of the end walls of the prototype building. The required structural performance is to maintain stability for 1 hour duration of exposure to the ASTM E119 [1] fire and to design-basis fires determined through applicable fire models. Alternatively, the acceptance criterion prescribed in the ASTM E119 standard for fire resistance rating of columns tested without applied loads is a maximum steel average temperature of 1,000 ºF (538 ºC) or maximum individual temperature of 1,200 ºF (649 ºC) [2].

2.4. Design loads

Loads on the structure and internal forces in the members of the end walls were determined from structural analysis using the applicable load combinations from ASCE 7 [4]. For the fire analysis and design, the load combination for extraordinary events is used. For the end walls of the prototype building, this combination leads to: $1.2\,Dead + 1.2\,Collateral + 0.2\,Snow$. (Note: there is no live load generating forces in the end wall structure because the columns support only a roof). Application of this load combination provides the required strength of the structure and its elements for LRFD.

The applied forces in the end wall columns in the fire situation are summarized in Table 3. As can be seen, the columns are only subjected to axial force in the fire situation, which results from the absence of horizontal loads in the combination.

Table 3 Applied design forces for LRFD in the end wall columns under the load combination applicable in the fire situation.

Location	Column	Axial force (k)	Shear force (k)	Moment (ft-k)
End wall framing line 1	EC-1	0.91	0	0
	EC-2	3.07	0	0
	EC-3	2.27	0	0
	EC-4	3.07	0	0
	EC-5	0.91	0	0
End wall framing line 7	EC-6	0.90	0	0
	EC-7	3.05	0	0
	EC-8	2.26	0	0
	EC-9	3.06	0	0
	EC-10	0.90	0	0

3. Design-basis fires

Besides the standard ASTM E119 fire curve, design-basis fire scenarios are also considered to assess the safety of the building in case of fire. The fire modeling software OZone [5] is used to calculate the gas temperature development in the warehouse. OZone relies on the zone model theory to evaluate the transient temperature and pressure in the compartment. The compartment is initially divided in two horizontal zones (pre-flashover), then it automatically transitions into a single zone after flashover. The differential equations that express the mass balance and the energy balance are numerically integrated on time. The temperature and pressure are considered as spatially uniform in each zone. The amount of combustible material present in the compartment (fire load), heat release rate (HRR), openings, thermal properties of the boundaries of enclosure, and propagation rate (slow, medium, or fast) are specified as inputs in the model.

3.1. Estimation of the fuel load density

The fuel load present in a compartment influences the severity of the fire. The fuel load is generally assumed based on tabulated data in standards, which provide statistics as a function of the building occupancy (e.g., Eurocode EN1991-1-2 [6], NFPA 557 [7]). However, values for storage facilities are not commonly reported. No value for such occupancy is provided in Eurocode nor in NFPA. The British BS 7974 Part 1 [8] provides values of fuel load density for manufacturing and storage occupancies, with average of 1,180 MJ/m^2 (103,905 Btu/ft^2), and the 80%, 90%, and 95% percentile at 1,800 MJ/m^2 (158,499 Btu/ft^2), 2,240 MJ/m^2 (211,332 Btu/ft^2), and 2,690 MJ/m^2 (236,868 Btu/ft^2), respectively. The large coefficient of variation reflects the fact that the fuel load in a storage facility depends heavily on the type of content stored. For a specific (existing) building, the fuel load can also be measured through surveying. Here, a conservative estimation of the fuel load density is carried out through a scenario-based assessment. The objective is to evaluate the most severe design-basis fire that could develop in the warehouse under the unfavorable situation where a fire occurs while the warehouse is full of combustible material.

The first step for the scenario-based estimation is to identify the type of material stored. The warehouse in this study is used to store moderate-hazardous materials. Based on the International Building Code (IBC) [3], moderate-hazardous materials include books, clothing, lumber, furs, leather, silks, and so on. The calorific values, H, of these materials are similar, slightly below 20 MJ/kg (8,598 Btu/lb), which was the conservative H value assumed for the fuel calculations.

Table 4 Net heat of combustion (net calorific value) of different materials [9].

Material	Calorific value, H ($\boldsymbol{MJ/kg}$)	Material	Calorific value, H ($\boldsymbol{MJ/kg}$)
Celluloid	18.5	Leather	19.0
Cellulose	18.1	Paper (average)	18.9
Cellulose triacetate	18.4	Paper, Cardboard	18.9
Clothes	20.2	Cotton	19.8
Material	Calorific value, H (BTU/lb)	Material	Calorific value, H (BTU/lb)
Celluloid	7950	Leather	8170
Cellulose	7780	Paper (average)	8130
Cellulose triacetate	7910	Paper, Cardboard	8130
Clothes	8680	Cotton	8510

The second step is to evaluate the amount of material present in the compartment. The volume of the warehouse is $75 \times 108 \times 12\ ft^3$. However, the warehouse cannot be fully filled with materials. The utilization ratio of the warehouse refers to how efficiently a warehouse is being made used of. A utilization ratio, r, of 25% is reported as typical and efficient to maximize storage while enabling operation, staff movement, etc. Based on that ratio, the volume of stored material cannot exceed: $V = r \cdot abc = 25\% \times 75 \times 108 \times 12\ ft^3 = 24{,}300\ ft^3$.

The average density of the stored content is assumed to be 550 kg/m^3 (34.3 lb/ft^3). This is the density of cross laminated timber (CLT) panels and is thus in line with the IBC classification of moderate-hazardous materials. The fuel load density can be obtained by multiplying the total mass of the stored content by its calorific value divided by the floor area A = 75 x 108 = 8,100 ft^2:

$$q = \frac{m \cdot H}{A} = \frac{\rho V \cdot H}{A} = \frac{0.55 \times 10^3\ kg/m^3 \times 24{,}300\ ft^3 \times 20\ MJ/kg}{8{,}100\ ft^2} = 9{,}900\ MJ/m^2$$

This is an upper bound of the fuel load density that could be present in the warehouse. This value is next compared to values from other sources. As mentioned above, the Eurocode [6] and NFPA 557 standard [7] do not specify the fuel load density for storage/warehouse occupancy, while the BS 7974 Part 1 [8] provides an average fuel load density for manufacturing and storage of 1,180 MJ/m^2 (103,905 Btu/ft^2) and a 95% percentile of 2,690 MJ/m^2 (236,868 Btu/ft^2). Table 5 gives fuel load density values from the British standard for different occupancies. In a recent survey of office rooms in Buffalo, New York, measured total fuel loads ranging from 368 to 3,451 MJ/m^2 (32,404 to 303,878 Btu/ft^2) were reported [10]. The scenario-based estimation of fuel load 9,900 MJ/m^2 (871,745 Btu/ft^2) is much higher than the values provided in these other sources. This is linked to the conservative assumption that 25% of the volume is filled with combustible material, based on the optimum utilization ratio of the storage room and assuming all the material present would be combustible and participate to the fire. In assessing the fire curves in the following sections, a sensitivity study of the influence of fuel load density is performed considering the value of 9,900 MJ/m^2 (871,745 Btu/ft^2) as the upper bound.

Table 5 BS 7974 Part 1: Fuel load density for typical occupancies [8].

Occupancy	Fuel load density			
	Average (MJ/m^2)	Fractile (MJ/m^2)		
		80 %	90 %	95 %
Dwelling	780	870	920	970
Hospital	230	350	440	520
Hospital storage	2,000	3,000	3,700	4,400
Hotel bedroom	310	400	460	510
Offices	420	570	670	760
Manufacturing	300	470	590	720
Manufacturing and storage	1,180	1,800	2,240	2,690
Libraries	1,500	2,250	2,550	-
Schools	285	360	410	450

Occupancy	Fuel load density			
	Average (BTU/ft^2)	Fractile (BTU/ft^2)		
		80 %	90 %	95 %
Dwelling	68,680	76,610	81,010	85,410
Hospital	20,250	30,820	38,740	45,790
Hospital storage	176,110	264,160	325,800	387,440
Hotel bedroom	27,300	35,220	40,500	44,910
Offices	36,980	50,190	59,000	66,920
Manufacturing	26,420	41,390	51,950	63,400
Manufacturing and storage	103,900	158,500	197,240	236,870
Libraries	132,080	198,120	224,540	-
Schools	25,100	31,700	36,100	39,620

3.2. Lining materials

Zone fire models include a wall model that captures the heat transfer between the air of the compartment and the surrounding walls, at the surface of the wall, inside the wall, then from the wall to the outside environment. It is possible to consider different types of walls, ceiling, and floor, possibly made of successive layers of different lining materials. Herein, the lining material of the walls is 5/8'' thick gypsum boards. The floor is 4'' thick normal weight concrete. The roof structure includes two layers of fiberglass insulation, 8'' and 3.5'' thick, as listed in Table 6.

Table 6 Lining materials in the warehouse.

Components	Lining materials
Wall	5/8'' gypsum boards
Floor	4'' normal weight concrete
Roof	8'' + 3.5'' fiberglass insulation

3.3. Openings

Zone fire models account for the transfer of mass through the openings. For this prototype building, the following openings are considered: one 3' x 7.5' opening at 0 ft sill height and eight 2.5' x 7.5'

openings at 4 ft sill height at the end wall framing line 1; four 10’ x 12’ openings and one 3’ x 7.5’ opening at 0 ft sill height at the side wall framing line A; and one 3’ x 7.5’ opening at 0 ft sill height at the side wall framing line E, as shown in Figure 3, Figure 4, Figure 6, and Figure 7.

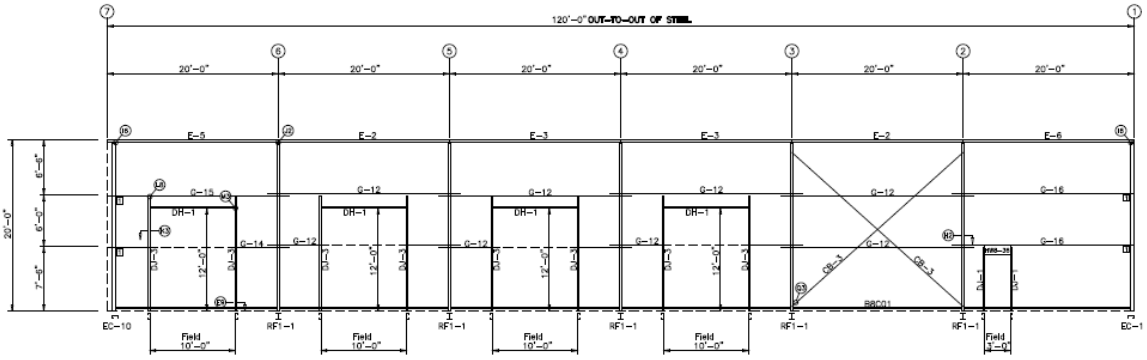

Figure 6 Side wall framing line A.

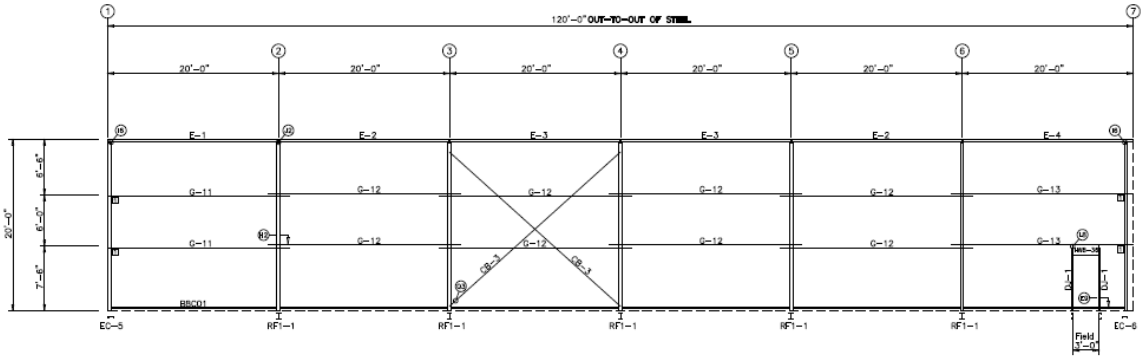

Figure 7 Side wall framing line E.

Table 7 Openings on the surrounding walls.

Wall	Dimensions of openings	Sill height (ft)
End wall framing line 1	3’ x 7.5’ and 8 x 2.5’ x 7.5’	0 and 4
End wall framing line 7	-	-
Side wall framing line A	4 x 10’ x 12’ and 3’ x 7.5’	0
Side wall framing line E	3’ x 7.5’	0

3.4. Fire curves determined from OZone model

The software OZone is used to evaluate the fire development in the warehouse based on the method in the Annex E of Eurocode 1991-1-2 [6]. The model assumes no active fire-fighting measures other than the presence of safe access routes, fire-fighting devices, and smoke exhaust system. The fire growth rate is assumed to be medium and the maximum heat release rate by 1 m^2 (10.8 ft^2) of fire in case of fuel-controlled condition, labelled RHR_f, is assumed to be 250 kW/m^2 (79,249 $Btu/(hr \cdot ft^2)$).

Given the uncertainty in the nature and amount of material stored, a sensitivity study is carried out on the fuel load, varying from 10% to 100% of the upper bound estimate of 9,900 MJ/m^2 (871,745 Btu/ft^2). It is assumed that the fire can develop over the full area of the warehouse

($75 \times 120\ ft$) and that half of the openings (i.e., windows and doors) are open for ventilation at the time of the fire. The gas temperatures obtained from OZone are plotted in Figure 8. The temperatures obtained using the fuel loads corresponding to different occupancies, as defined in the Eurocode, are also plotted for comparison. The ASTM E119 fire curve is also shown. As can be seen, the temperatures from the OZone models with different fuel loads follow a similar trend for the heating phase. Indeed, the heating phase is governed by the fire growth rate and the available oxygen. The fuel load influences the fire duration, with larger fuel loads leading to longer fires. In contrast with the OZone fires, the ASTM E119 curve is a post-flashover curve, which heats up very fast without capturing the incipient and growing phases of the fire. As a result, within the 1-hour duration of interest, the ASTM E119 curve is more severe than the design-basis fires obtained through modeling.

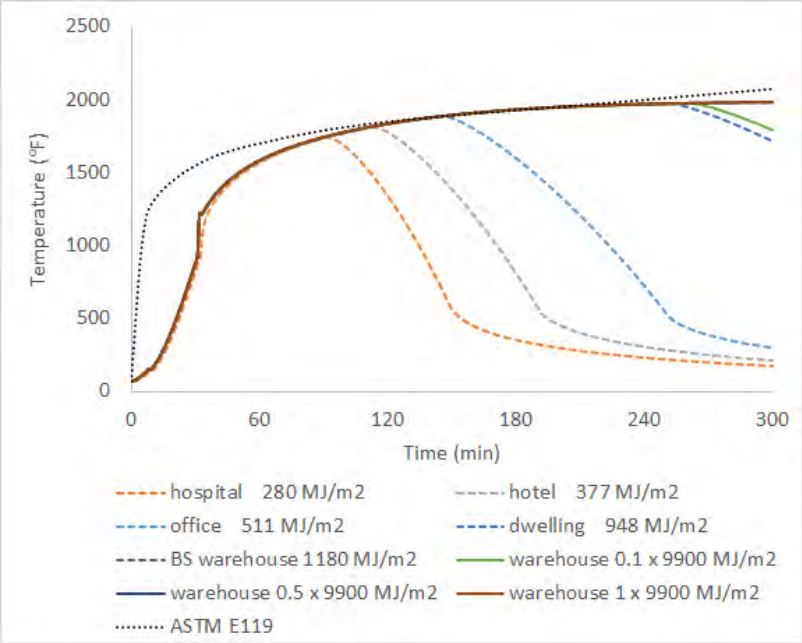

Figure 8 Gas temperature with fire developing over the full warehouse area and openings 50% open for ventilation.

The influence of ventilation is analyzed by changing the assumption on the openings. In Figure 9, the fire curves were obtained assuming that all the windows and doors present in the building were fully open (100% of possible openings are open). It can be observed that with more air coming inside the warehouse for the combustion, the temperatures reach a higher peak in a shorter time. Due to the limited fuel load, the descending branch starts at a shorter time.

Two other cases, in which only the area for storage ($75 \times 105 \times 12\ ft$) is exposed to fire, are explored, as shown in Figure 10 and Figure 11. Similar observations can be found that the case with openings 50% open for ventilation yields longer, but cooler fire curves, while the case with openings 100% open for ventilation yields shorter, but hotter fire curves.

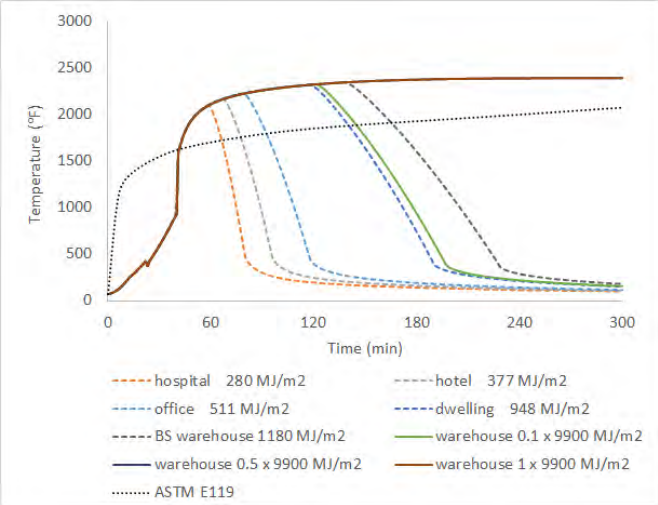

Figure 9 Gas temperature with fire developing over the full warehouse area and openings 100% open for ventilation.

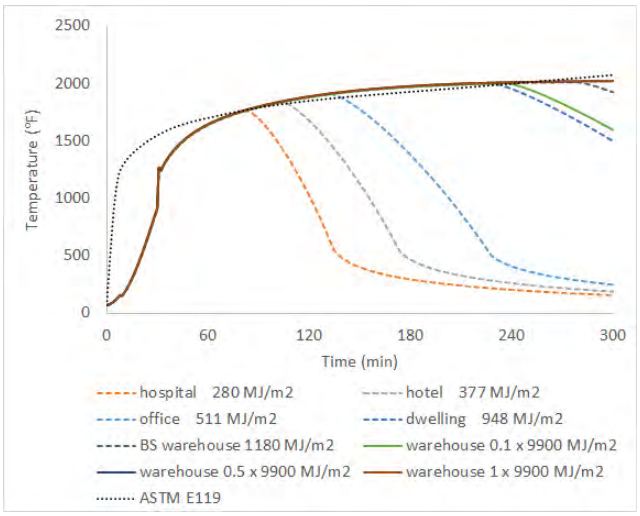

Figure 10 Gas temperature with fire developing over the storage area and openings 50% open for ventilation.

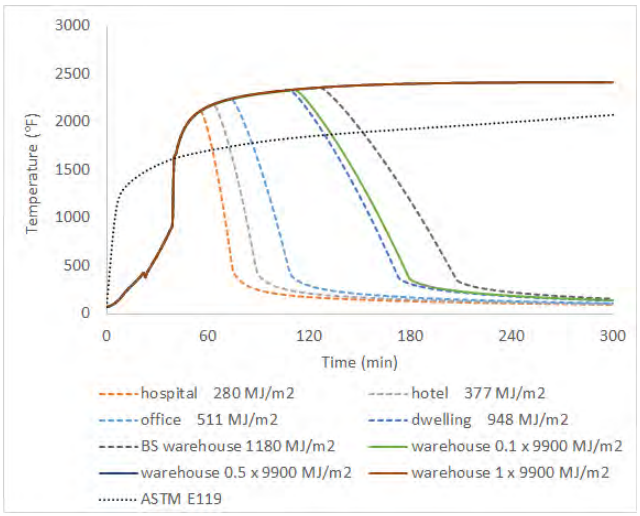

Figure 11 Gas temperature with fire developing over the storage area and openings 100% open for ventilation.

4. Thermal analysis of cold-formed steel columns

4.1. Fire protection assemblies

The cold-formed steel columns, comprised of one or two C-shapes, at the end wall frame line 1 and 7 are thermally protected according to applicable fire-resistance-rated assemblies for 1-hour duration. The fire protection enclosure is based on the 1-hour rated UL X530 design with 2 layers of 5/8-inch Type X gypsum board, as summarized in Table 8. The different fire protection configurations (N1, N2, and N3) derived from this reference assembly and used in this project are shown in Figure 12. The double C-shape columns are designated as N1 and N3.

Table 8 Fire protection configuration of the cold-formed steel columns.

Location	Column	Fire protection	
End wall framing line 1	EC-1	UL X530	[1 HR]
	EC-2	X530-N2	[1 HR]
	EC-3	X530-N3	[1 HR]
	EC-4	X530-N2	[1 HR]
	EC-5	UL X530	[1 HR]
End wall framing line 7	EC-6	UL X530	[1 HR]
	EC-7	UL X530	[1 HR]
	EC-8	X530-N1	[1 HR]
	EC-9	UL X530	[1 HR]
	EC-10	UL X530	[1 HR]

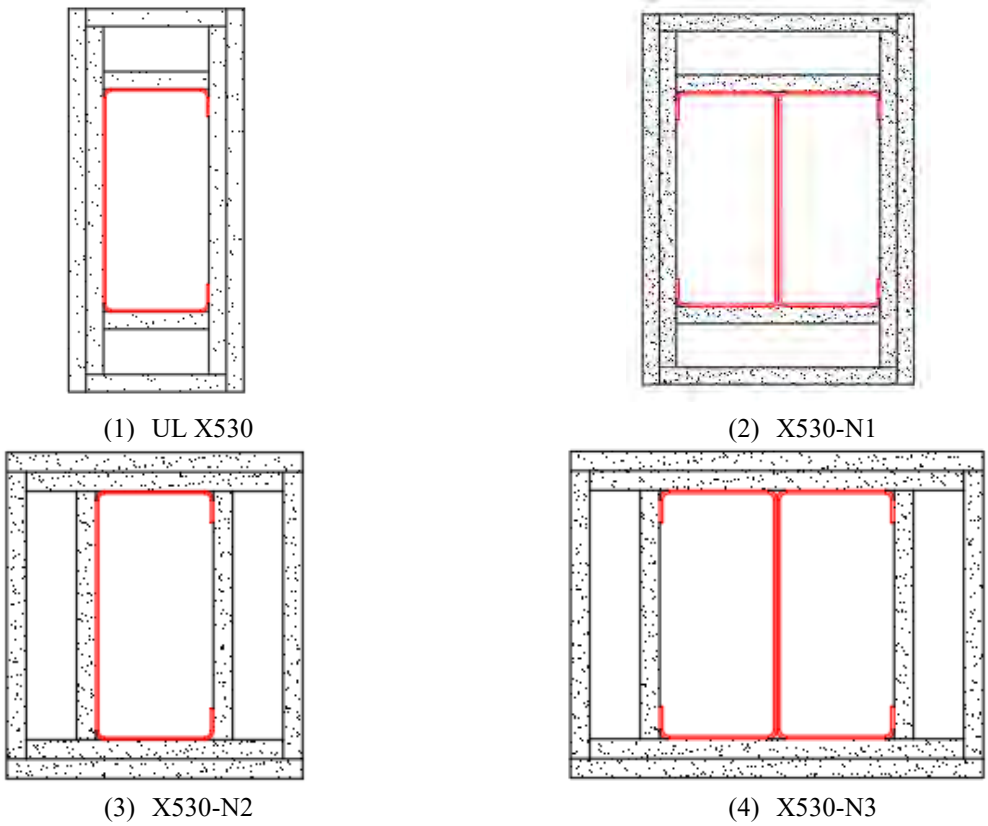

(1) UL X530 (2) X530-N1

(3) X530-N2 (4) X530-N3

Figure 12 Fire protection design of the columns.

4.2. Thermal properties

The finite element software SAFIR [11] is used to carry out the thermal analysis using temperature-dependent material properties. Thermal properties of the steel are taken from Eurocode EN1993-1-2, as shown in Figure 13.

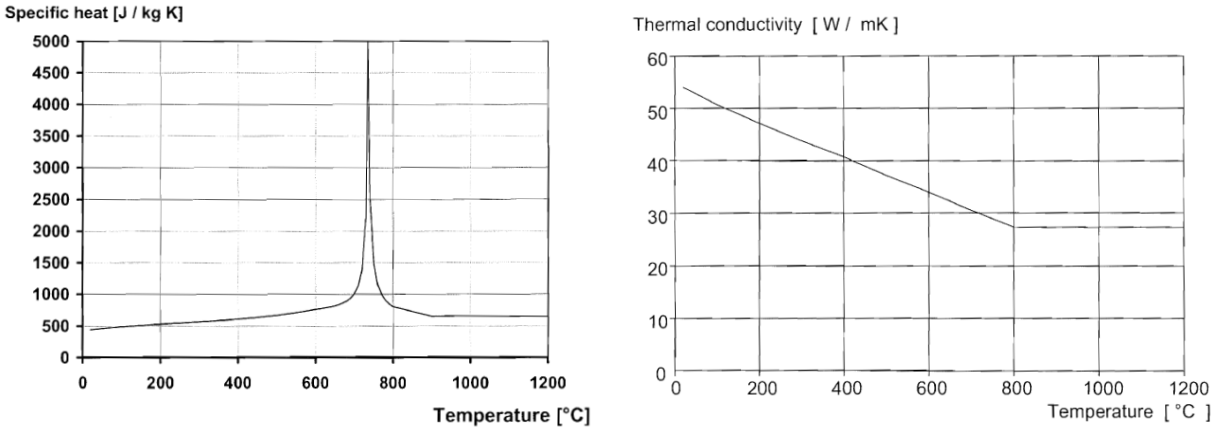

(1) Specific heat (2) Thermal conductivity

Figure 13 Thermal properties of steel.

Thermal properties of the Type X gypsum board are based on the research by Cooper [12]. The thermal properties are shown in Figure 14. The properties provided by Cooper originated from Sultan's [18] work at the NRC Canada on Type X boards. The density of the Type X gypsum is taken as 648 kg/m^3 (40.4 lb/ft^3) at ambient temperature.

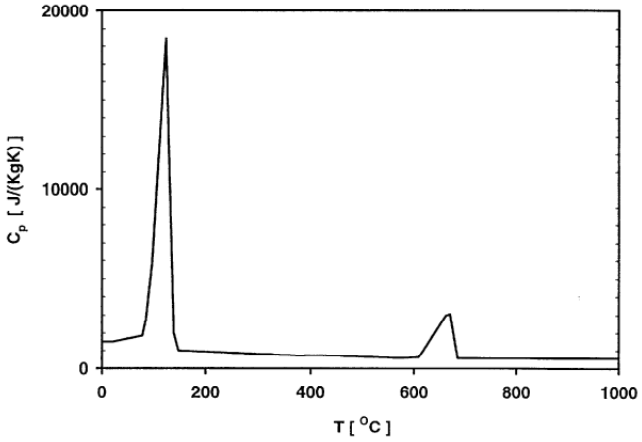

(1) Specific heat

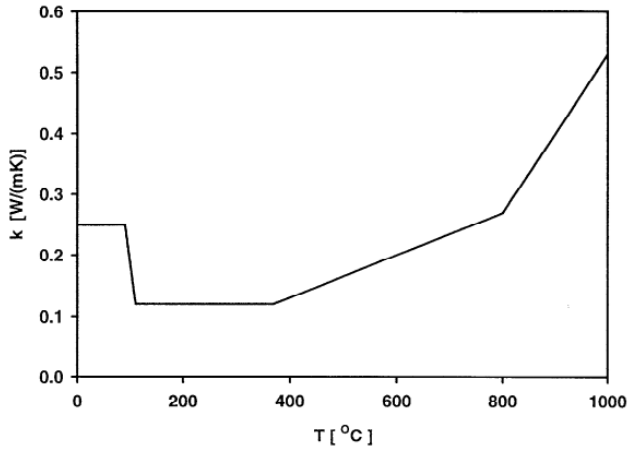

(2) Thermal conductivity

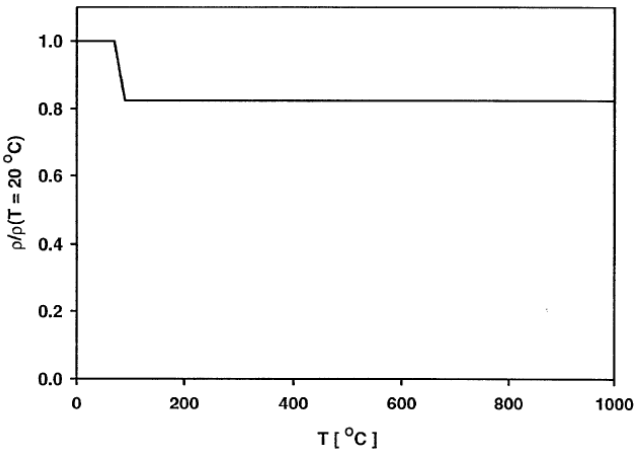

(3) Density

Figure 14 Thermal properties of gypsum board.

4.3. Finite element model

The protected columns are modeled using 4 elements across the thickness of each gypsum board layer. The columns are exposed to the ASTM E119 fire or design-basis fires on all 4 sides, as shown in Figure 15. The radiation and convection within the cavities of the assemblies are taken into account. The emissivity of the gypsum board is taken as 0.8. The convective coefficient is taken as 25 W/m^2K (4.4 $Btu/(hr \cdot ft^2 \cdot °F)$) for columns subjected to ASTM E119 fire or 35 W/m^2K (6.2 $Btu/(hr \cdot ft^2 \cdot °F)$) for those subjected to design-basis fires, according to Eurocode EN1991-1-2. The steel studs, screws, and corner bead are not modeled.

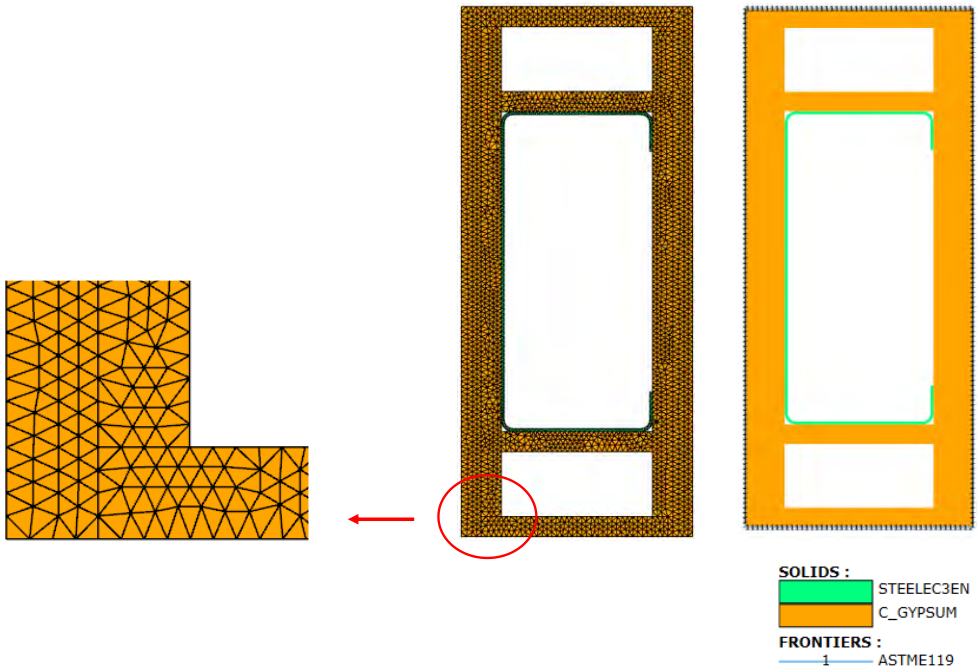

Figure 15 Finite element model of columns subjected to fire on 4 sides.

4.4. Thermal analysis of columns subjected to ASTM E119 fire

The temperature history in the flange and web of the EC-6/ EC-10 columns is shown in Figure 16. It can be observed that the temperature is generally uniform. At 60 minutes, the temperature in the flange and web is 499 °C (930 °F) and 497 °C (927 °F), respectively. The temperature in the flange and web of each column at 60 minutes is summarized in Table 9. The temperature distributions of each column assembly at 60 minutes are shown in Appendix A. The temperature in the steel profile is approximately uniform, except a relatively larger discrepancy is observed in the double C-shaped sections EC-3 and EC-8.

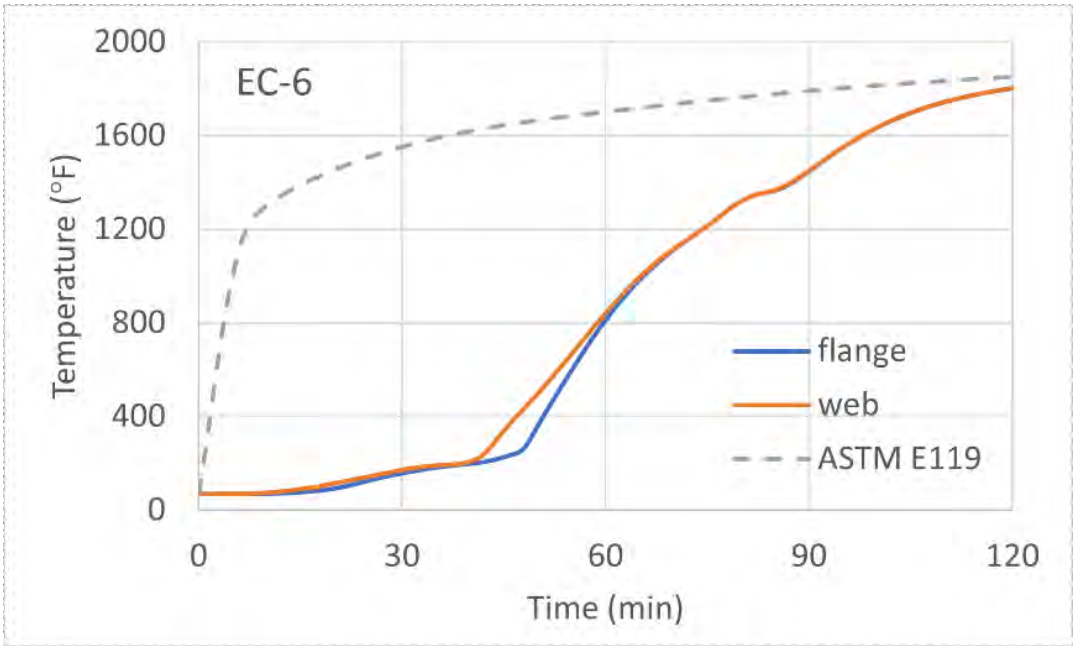

Figure 16 Temperature in the flange and web of EC 6/EC 10 subjected to ASTM E119 fire.

Table 9 Steel temperature in the end wall columns at 60 minutes under ASTM E119 fire.

Location	Column	Flange (°F/°C)	Web (°F/°C)
End wall framing line 1	EC-1	887 / 475	892 / 478
	EC-2	707 / 375	712 / 378
	EC-3	656 / 347	576 / 302
	EC-4	790 / 421	799 / 426
	EC-5	887 / 475	892 / 478
End wall framing line 7	EC-6	930 / 499	927 / 497
	EC-7	747 / 397	743 / 395
	EC-8	651 / 344	567 / 297
	EC-9	851 / 455	855 / 457
	EC-10	930 / 499	927 / 497

4.5. Thermal analysis of columns subjected to design-basis fires

The temperatures in the flange and web of each column at 60 minutes under design-basis fires are summarized in Table 10 to Table 13. The OZone fire is labelled in the form of the dimension of the compartment exposed to fire and percentage of openings that are open for ventilation. For example, 'OZone fire _Entire floor_50%' refers to the case in which the fire can develop over the full surface area of the warehouse, and 50% openings are open for ventilation. 'OZone fire _Warehouse ara_100%' refers to the case in which only the storage area is exposed to fire, and 100% openings are open for ventilation.

It can be observed that the temperature of the columns subjected to the design-basis fires are still moderate after 60 minutes of exposure. The effect of these temperatures, below 350 °F, on the capacity is not significant. In particular, the temperatures after 60 minutes under the design-basis fires are much lower than those under the ASTM E119 fire. This results from the faster rate of temperature increase in the early stage of the time-temperature curve with the ASTM E119 fire, as discussed in Section 3. Therefore, the mechanical analysis in the next section focuses only on the columns subjected to the ASTM E119 fire.

Table 10 Temperature in the end wall columns at 60 minutes under OZone fire_Entire floor_50%.

Location	Column	Flange (°F/°C)	Web (°F/°C)
End wall framing line 1	EC-1	198 / 92	196 / 91
	EC-2	198 / 92	192 / 89
	EC-3	192 / 89	169 / 76
	EC-4	199 / 93	192 / 89
	EC-5	198 / 92	196 / 91
End wall framing line 7	EC-6	198 / 92	198 / 92
	EC-7	190 / 88	198 / 92
	EC-8	181 / 83	160 / 71
	EC-9	196 / 91	205 / 96
	EC-10	198 / 92	198 / 92

Table 11 Temperature in the end wall columns at 60 minutes under OZone fire_Entire floor_100%.

Location	Column	Flange (°F/°C)	Web (°F/°C)
End wall framing line 1	EC-1	248 / 120	194 / 90
	EC-2	212 / 100	190 / 88
	EC-3	210 / 99	160 / 71
	EC-4	217 / 103	192 / 89
	EC-5	248 / 120	194 / 90
End wall framing line 7	EC-6	194 / 90	270 / 132
	EC-7	194 / 90	221 / 105
	EC-8	187 / 86	161 / 72
	EC-9	199 / 93	248 / 120
	EC-10	194 / 90	270 / 132

Table 12 Temperature in the end wall columns at 60 minutes under OZone fire_Warehouse area_50%.

Location	Column	Flange (°F/°C)	Web (°F/°C)
End wall framing line 1	EC-1	203 / 95	201 / 94
	EC-2	203 / 95	198 / 92
	EC-3	174 / 79	198 / 92
	EC-4	205 / 96	198 / 92
	EC-5	203 / 95	201 / 94
End wall framing line 7	EC-6	201 / 94	205 / 96
	EC-7	198 / 92	205 / 96
	EC-8	189 / 87	167 / 75
	EC-9	201 / 94	210 / 99
	EC-10	201 / 94	205 / 96

Table 13 Temperature in the end wall columns at 60 minutes under OZone fire_Warehouse area_100%.

Location	Column	Flange (°F/°C)	Web (°F/°C)
End wall framing line 1	EC-1	266 / 130	199 / 93
	EC-2	221 / 105	198 / 92
	EC-3	221 / 105	162 / 72
	EC-4	230 / 110	198 / 92
	EC-5	266 / 130	199 / 93
End wall framing line 7	EC-6	207 / 97	316 / 158
	EC-7	198 / 92	246 / 119
	EC-8	192 / 89	169 / 76
	EC-9	205 / 96	288 / 142
	EC-10	207 / 97	316 / 158

5. Mechanical analysis of cold-formed steel columns

According to the proposed Appendix 4 to AISI S100 [1], the evaluation of the performance of cold-formed steel structural members at elevated temperatures during exposure to fire can be performed using simple methods or advanced methods of analysis. Herein, the fire performance of the cold-formed steel columns from the end walls is evaluated with the Direct Strength Method (DSM) as an application of a simple analytical method, and with finite element modeling (FEM), as an application of an advanced numerical method.

5.1. Analysis by Direct Strength Method/AISI S100

The Direct Strength Method (DSM) [13] and AISI S100 [1] is used to assess the loadbearing stability of the columns under fire exposure. For members subjected to uniform and near-uniform temperature distribution, as is the case here, the ambient temperature design capacity rules can be used with reduced mechanical properties at elevated temperature.

The DSM directly integrates the elastic buckling analysis in the design and uses the gross cross-sectional properties. The column design rules of DSM that consider the global, local, and distortional buckling at elevated temperatures are shown in Eq. (1). Detailed calculations of each buckling strength are provided for two columns in Appendix C and Appendix D.

$$P_{DSM} = \min(P_{ne}, P_{nl}, P_{nd}) \quad (1)$$

where P_{ne} is the nominal axial strength for overall buckling (i.e., flexural, torsional, or flexural–torsional); P_{nl} is the nominal axial strength for local buckling; and P_{nd} is the nominal axial strength for distortional buckling. The DSM is a procedure within the AISI S100 that provides nominal values of the strength. For fire design, the nominal strength values are considered the same as the design strength in the LRFD, because the resistance factor is taken as 1.0. Therefore, the nominal strength calculated with the DSM is compared to the required strength determined from the gravity load combination defined in Section 2.4.

5.1.1. Capacity of the columns at ambient temperature by DSM/AISI S100

The capacities of the columns at ambient temperature evaluated by DSM are given in Table 14. The double C-shaped columns EC-3 and EC-8 were not structurally designed as an interconnected member but as two individual single C-shaped columns. Thus, the listed capacity for EC-3 and EC-8 is twice that of an individual single C-shaped column. The failure mode at ambient temperature is local buckling for all columns. The load ratio is provided as the ratio between the required strength in the fire situation (see Section 2.4) and the available strength (taken as the nominal strength value evaluated by DSM, as the resistance factor is taken as 1.0 for fire design). This load ratio is lower than 10%, meaning the columns have significant reserve in strength at the time the fire starts. It is worth noting that the load combination applicable in a fire does not include wind load, which is the dominant load for column design at ambient temperature. The columns are not oversized for ambient temperature design, but when considering the load combination for the fire situation, the demand over capacity is initially low.

Table 14 Capacity of the columns at ambient temperature as evaluated by DSM.

Location	Columns	DSM (kip)	Load ratio Load[b] / DSM
End wall framing line 1	EC-1/EC-5	21.0 (L[a])	0.04
	EC-2	45.6 (L)	0.06
	EC-3	31.5 (L)	0.07
	EC-4	36.2 (L)	0.08
End wall framing line 7	EC-6/EC-10	21.0 (L)	0.04
	EC-7	45.6 (L)	0.06
	EC-8	31.5 (L)	0.07
	EC-9	36.2 (L)	0.08

Note: [a]'L' refers to local buckling. [b]'Load' refers to the applied load under load combination applicable in the fire situation (from ASCE 7).

5.1.2. Capacity of the columns at elevated temperature by DSM/AISI S100

The mechanical properties of the steel decreases at elevated temperature, resulting in lower capacity of the columns in fire. Based on the results of the heat transfer analysis, the temperature in the cross section of the columns is approximately uniform after 60 minutes of exposure to ASTM E119. Accordingly, the steel temperature is assumed as uniform and taken at the maximum value across the steel cross section. The temperature-dependent reduction relationships for the mechanical properties of cold-formed steel are provided in Appendix B, which are included in the proposed Appendix 4 to AISI S100. The capacity of the columns at 60 minutes under ASTM E119, evaluated with the DSM considering the reduction of mechanical properties in fire, are given in Table 15. The calculations show that the capacity of the columns at 60 minutes is still significantly larger than the demand; the demand-to-capacity ratio does not exceed 15%. As a result, the analysis based on the DSM shows that the 1-hour fire-resistance-rated assemblies for the end wall columns do indeed maintain stability for much longer than 1 hour under fire.

Table 15 Capacity of the columns at 60 minutes subjected to ASTM E119 by DSM.

Location	Columns	Temperature (°F / °C)	DSM (kip)	Load ratio Load[b] / DSM
End wall framing line 1	EC-1/EC-5	892 / 478	10.8 (L[a])	0.09
	EC-2	712 / 378	32.0 (L)	0.10
	EC-3	656 / 347	23.9 (L)	0.10
	EC-4	799 / 426	22.2 (L)	0.14
End wall framing line 7	EC-6/EC-10	930 / 499	10.0 (L)	0.09
	EC-7	747 / 397	30.3 (L)	0.10
	EC-8	651 / 344	24.0 (L)	0.09
	EC-9	855 / 457	20.0 (L)	0.15

Note: [a]'L' refers to local buckling. [b]'Load' refers to the applied load under load combination applicable in the fire situation (from ASCE 7).

5.1.3. Failure temperature and failure time by DSM/AISI S100

The failure temperature can be obtained by searching for the temperature at which the column demand-to-capacity load ratio becomes equal to 1. The procedure is as follows: 1) Input the section temperature; 2) Calculate the resulting retention factors (Appendix B); 3) Calculate the capacity at that temperature with DSM; 4) Evaluate the utilization ratio as demand / capacity; 5) Find the failure temperature by iteratively repeating steps 1-4 until the utilization ratio is equal to 1; 6) Find the failure time from the finite element thermal analysis as the time at which the failure temperature is reached.

The failure temperatures and failure times of each column are given in Table 16. The failure temperatures are high at approximately double the steel temperatures reached after 60-minutes of the fire exposure, which results from the low values of the load ratio in Table 15 at that time exposure for these end wall columns. Based on the thermal analysis discussed in Section 4, the failure time of a column is taken as the time step when the corresponding column reaches the failure temperature. It can be observed that the failure time of each column is much longer than 60 minutes, indicating that the columns satisfy the fire resistance rating and achieve stability under the ASTM E119 fire for a least 1 hour. The longest failure times occurred for the double C-shaped columns EC-3 and EC-8, whose loadbearing stability was maintained for more than 2 hours.

Table 16 Failure temperature and failure time by DSM for ASTM E119 fire.

Location	Columns	Failure time (minutes)	Failure temperature (°F/°C)
End wall framing line 1	EC-1/EC-5	116	1,794 / 979
	EC-2	116	1,672 / 911
	EC-3	127	1,657 / 903
	EC-4	101	1,582 / 861
End wall framing line 7	EC-6/EC-10	116	1,798 / 981
	EC-7	116	1,674 / 912
	EC-8	127	1,659 / 904
	EC-9	100	1,584 / 862

5.2. Analysis by finite element modeling

The structural stability of the end wall columns is also assessed by finite element modeling. Shell finite elements are used in the nonlinear FE software SAFIR [11] to analyze the behavior of the columns under fire exposure. The elements are quadrilateral nonlinear thin shell elements. The length of the columns in the model is 7.5 ft. The mesh size is $10\ mm \times 20\ mm$ ($0.4\ in\ \times 0.8\ in$). The boundary condition is pinned-pinned, as shown in Figure 17. The load is applied on an end plate at the top of the column to allow uniform distribution of the load. Both global imperfections and local imperfections are included in the model through modification of the initial coordinates of the nodes in the model of the columns to give initial deformed shapes that follow the buckling eigenmodes. An elastic buckling analysis is carried out in Abaqus, and global imperfections are applied according to the deformed shape of the global eigenmode with a maximum magnitude of $L/1000$ (L is the unbraced length). Local imperfections are applied according to the web and flange eigenmode for local buckling with a maximum magnitude of $b/200$ (where b is the width of flange for flange eigenmode, and the depth of web for web eigenmode). These local imperfections are scaled to 70% as recommended in the Eurocode EN1993-1-5 for combination

of global and local modes. The eigenmodes obtained from Abaqus for the column EC-6 are shown in Figure 18.

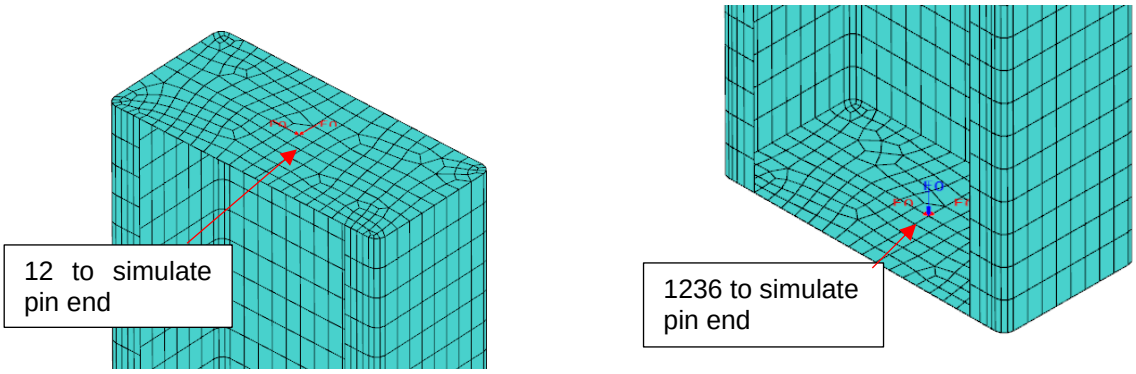

(1) Loading end (2) Supporting end

Figure 17 Boundary conditions of pinned-ended columns.

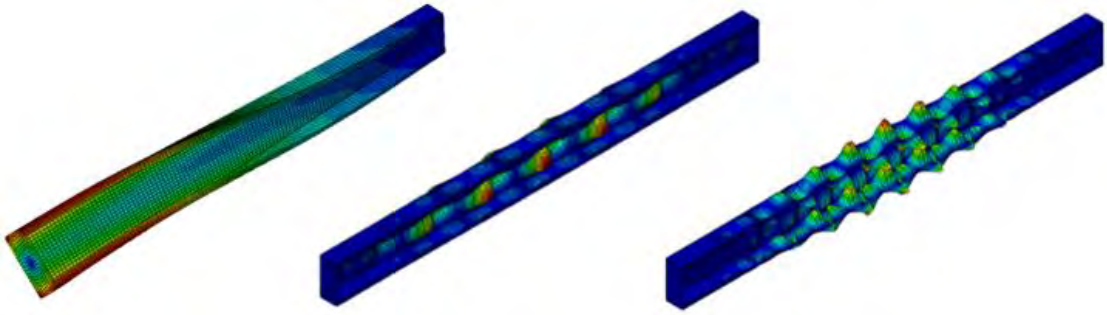

Global Local: web Local: flange

Figure 18 Global and local eigenmodes obtained by Abaqus.

5.2.1. Capacity of the columns at ambient temperature by FE analysis

The capacity of the columns at ambient temperature are evaluated with the FE model by increasing the load to failure. Structural failure is defined as the last converged time step, i.e., failure is deemed to occur when the implicit nonlinear analysis cannot find a stable converged solution. Runaway out-of-plane displacements associated with instability are observed at that time. Results are given in Table 17. These capacities obtained by FE analysis can be compared with the capacities obtained by application of the DSM method, listed in Table 14. The capacity obtained with the two methods agree very well with relative differences of only about 5%. The DSM generally provides slightly lower estimates (conservative) of the ambient temperature capacity than the FE analysis, except for the EC-4 and EC-9 columns, which are deeper open section columns. The deformed shape at failure of the columns is shown in Figure 19. The columns generally fail by interaction of local buckling in the web and flange and distortional buckling.

Table 17 Capacity of the columns at ambient temperature by FE analysis and DSM.

Location	Columns	DSM (kip)	SAFIR/Shell FE (kip)
End wall framing line 1	EC-1/EC-5	21.0	22.1
	EC-2	45.6	47.9
	EC-3	31.5	33.7
	EC-4	36.2	34.6
End wall framing line 7	EC-6/EC-10	21.0	22.1
	EC-7	45.6	47.9
	EC-8	31.5	33.7
	EC-9	36.2	34.6

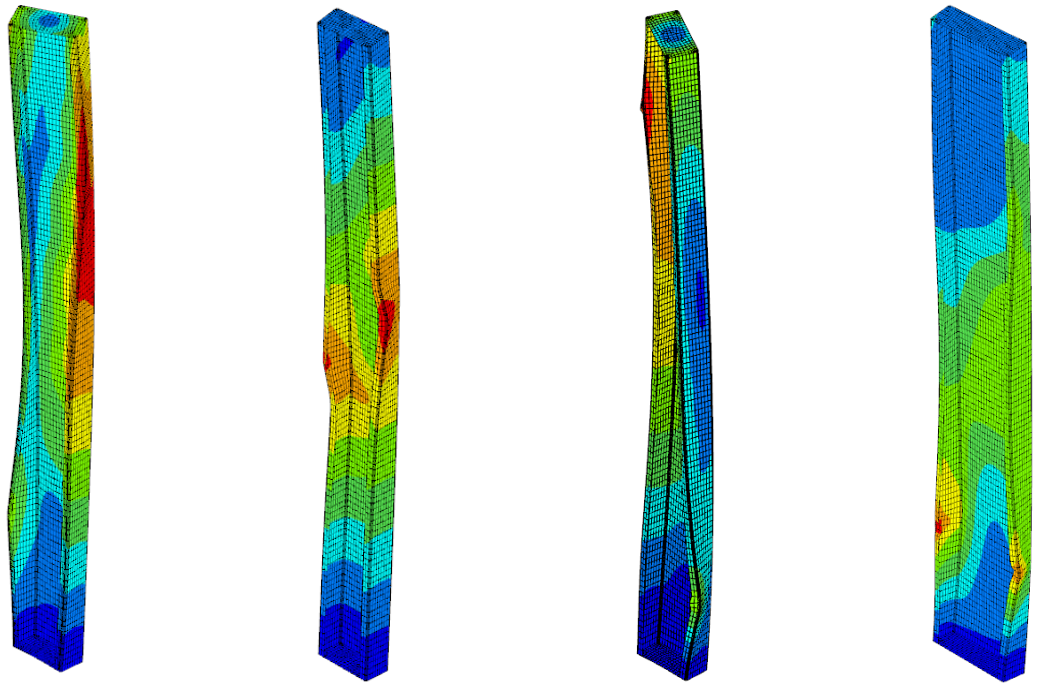

EC-1/EC-5 EC-6/EC-10 | EC-2 EC-7 | EC-3 EC-8 | EC-4 EC-9

Figure 19 Failure modes of columns at ambient temperature.

5.2.2. Failure temperature and failure time by FE analysis

The failure time for each column is computed with the FE model by applying the applicable load under load combination for fire and letting the member temperature increase according to the heat transfer analysis results for the ASTM E119 standard fire. The software allows automatic coupling of the heat transfer outputs into the mechanical analysis. Results of failure time and failure temperature are given in Table 18. The results obtained from the FE analysis agree with those obtained from application of the DSM procedure in AISI S100. For EC-1, EC-5, EC-6 and EC-10, the simulation stopped when the member temperature reached 1,000 °C (1,832 °F), because this is the upper limit of applicability of the steel mechanical property models proposed in AISI S100 [1]. Therefore, the failure temperatures of these columns are marked as '1,000+'. The results from the

FE analysis confirm that the end wall columns maintain stability well over 1 hour under the standard fire.

Table 18 Failure temperature and failure time by FEM analysis for ASTM E119 fire

Location	Columns	DSM		SAFIR/Shell FE	
		Failure time (min)	Failure temperature (°F/°C)	Failure time (min)	Failure temperature (°F/°C)
End wall framing line 1	EC-1/EC-5	116	1,794 / 979	120+	1,832+ / 1,000+
	EC-2	116	1,672 / 911	113	1,629 / 887
	EC-3	127	1,657 / 903	126	1,650 / 899
	EC-4	101	1,582 / 861	98	1,524 / 829
End wall framing line 7	EC-6/EC-10	116	1,798 / 981	120+	1,832+ / 1,000+
	EC-7	116	1,674 / 912	112	1,632 / 889
	EC-8	127	1,659 / 904	127	1,652 / 900
	EC-9	100	1,584 / 862	96	1,526 / 830

6. Verification of the fire performance of the metal steel building end walls

Sections 3 to 5 have evaluated through analysis the design-basis fires, thermal response, and mechanical response at elevated temperature of the cold-formed steel columns that compose the end walls of the prototype buildings. The required structural performance for these columns was to maintain loadbearing stability for 1 hour duration of exposure to fire.

The thermal analysis based on finite element modeling has shown that consideration of the ASTM E119 fire led to higher temperatures in the steel members at 60 minutes than other design-basis fires, even with very large values of fuel loads, because the latter had a slower growth phase at the early stage. Therefore, verification of the column stability was made using the ASTM E119 fire. The temperature in the steel remained lower than 930 °F (500 °C) at 60 minutes due to the fire protection. The temperature in the C-shaped steel members is approximately uniform.

The mechanical analysis was performed using two methods: the DSM procedure in AISI S100 and finite element modeling. Both methods demonstrate that the required performance is achieved, i.e., the columns maintain their loadbearing stability for more than 60 minutes of the standard fire exposure. The DSM calculates the nominal strength (capacity) at 60 minutes considering the reduction in steel mechanical properties at high temperatures. The demand-to-capacity ratio between this elevated temperature capacity at 60 minutes and the loading resulting from the applicable load combination from ASCE 7 does not exceed 15%. This is mainly because the applicable load combination for fire does not include wind, and therefore the columns are subjected to low force demands as compared with their capacity. The FE analysis calculates the time of failure for the columns subjected to the applicable loading and the transient temperature increase from the fire. The failure time exceeds 90-minutes for all columns and even reached 2-hours for half of the columns. This suggests possibility of optimizing the fire protection design strategy for the end wall members in this specific building prototype.

In conclusion, application of the analysis method according to the proposed Fire Appendix to AISI S100 to the case of the end wall columns for the prototype building allowed explicitly demonstrating satisfactory performance of the cold-formed steel assemblies. The columns can maintain stability for over one hour of fire exposure.

7. Fire rating of assemblies based on limiting steel temperature

The previous sections have focused on a specific prototype structure, for which stability of cold-formed steel members and assemblies can be checked at specific duration of fire exposure considering the applied loading, geometry, boundary conditions, etc. In this section, a generic situation is considered. The objective is to apply the analysis method to evaluate the performance of different fire protection assemblies in terms of the limiting steel temperature criteria at 60 minutes of standard fire exposure. Such analysis is useful notably to evaluate assemblies that have not been fire-rated through standardized physical testing, as is the case of the double-C shapes used for columns EC-3 and EC-8 in the prototype building.

7.1. ASTM E119 standard fire testing

As an alternative test procedure to evaluate the adequacy of the fire protection of steel columns without application of loading, the column should be exposed to the standard ASTM E119 fire curve, as shown in Figure 20, on all sides for the full member length. The temperature should be measured at four levels with no fewer than three thermocouples at each level. The condition of acceptance is that:

1) the transmission of heat through the protection during the period of fire exposure for which classification is desired does not raise the average (arithmetical) temperature of the steel at any one of the four levels above 1,000 °F (538 °C); and

2) does not raise the temperature above 1,200 °F (649 °C) at any one of the measured points.

This test method, based only on the thermal response of the member and its fire protection, is commonly used for standard (prescriptive) fire resistance rating of column assemblies. The critical temperatures indirectly account for the structural/mechanical response of the column during the fire by limiting the steel strength degradation to no more than approximately 50% of its ambient value.

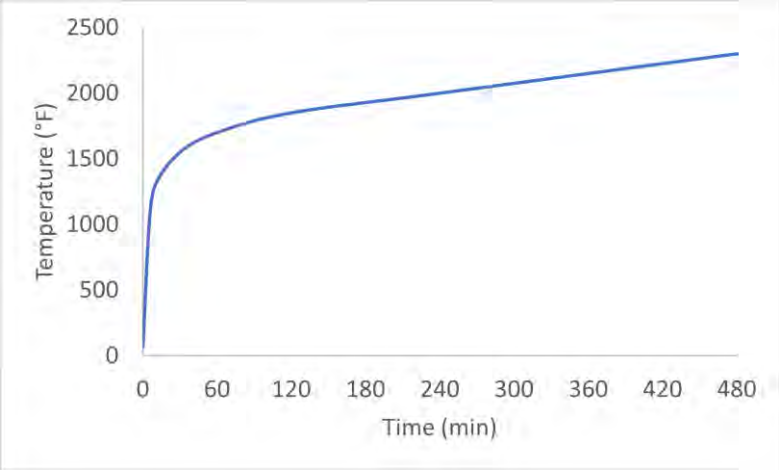

Figure 20 Time temperature curve of ASTM E119 fire.

7.2. Thermal analysis of columns with different fire protection assemblies

This section presents results of thermal analyses of assemblies to evaluate the temperature distribution and the time at which the limiting steel temperature criteria is reached. Type X gypsum boards are used. Thermal properties for the Type X gypsum are those given in Figure 14, adopted from Cooper [12]. Five different fire protection assemblies are analyzed. The number of layers and thickness of the Type X gypsum boards are as follows and as shown in Figure 21:

- 1 layer of 1'' gypsum
- 2 layers of ½'' gypsum
- 2 layers of 5/8'' gypsum
- 3 layers of 5/8'' gypsum
- 2 layers of 1'' gypsum

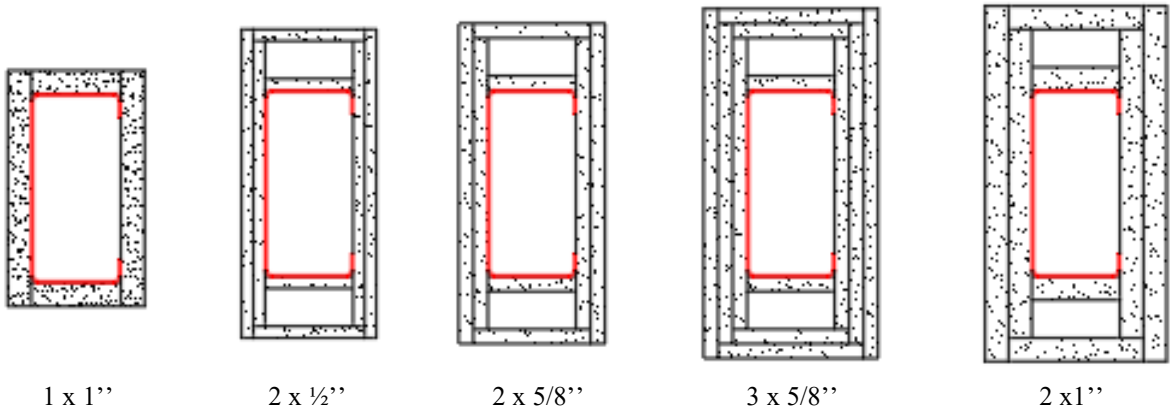

Figure 21 Fire protection assemblies considered in the analysis. Type X gypsum boards are used.

Thermal analyses are carried out in SAFIR for the five fire protection assemblies applied to each column of the end walls. The average steel temperatures at 60 minutes and 120 minutes under ASTM E119 fire are given in Table 19. The temperature distribution on the cross section of the EC-6 and EC-8 columns can be found in Appendix E.

For the 1-hour rating, the proposed Type X assembly based on UL X530 (i.e., 2 layers of 5/8'' gypsum) satisfies the limiting temperature criteria as evaluated through thermal analysis. For the double C-shaped section EC-8, the 1-hour rating can be achieved using 2 layers of ½'' gypsum. This represents a reduction in the thickness of the gypsum boards as compared with what is required for single C-shaped sections for the same fire rating. This is due to the more favorable section factor of the double C-shaped section, which results in the lower steel temperatures as quantified by the heat transfer analysis.

For the 2-hour rating, the proposed Type X assembly based on UL X530 (3 layers of 5/8'' gypsum) did not satisfy the limiting temperature criteria as evaluated through thermal analysis. This divergence between the outcomes of the standard fire test and the analysis is likely due to the assumed thermal properties of the gypsum board for the analysis being different than those of the Type C gypsum board used in the fire test. A parametric study on the thermal properties of gypsum is carried out in the following section. The columns EC-7 and EC-8 with 2 layers of 1'' Type X gypsum satisfy the thermal requirements for 2-hour rated assembly.

Table 19 Average steel temperatures at 60 minutes and 120 minutes under ASTM E119 fire. Type X gypsum boards used in the assemblies.

Temperatures in (°C)

column	1 x 1''		2 x ½''		2 x 5/8''		3 x 5/8''		2 x 1''	
	1h	2h	1h	2h	1h	2h	1h	2h	1h	2h
EC-6/EC-10	716	1001	705	1001	**499**	990	**87**	718	**81**	621
EC-7	620	988	607	989	**397**	937	**82**	625	**76**	**533**
EC-8	556	960	**535**	960	**344**	857	**70**	558	**71**	**476**
EC-9	671	998	661	998	**457**	974	**85**	670	**80**	583

Temperatures in (°F)

column	1 x 1''		2 x ½''		2 x 5/8''		3 x 5/8''		2 x 1''	
	1h	2h	1h	2h	1h	2h	1h	2h	1h	2h
EC-6/EC-10	1321	1834	1301	1834	**930**	1814	**189**	1324	**178**	1150
EC-7	1148	1810	1125	1812	**747**	1719	**180**	1157	**169**	**991**
EC-8	1033	1760	**995**	1760	**651**	1575	**158**	1036	**160**	**889**
EC-9	1240	1828	1222	1828	**855**	1785	**185**	1238	**176**	1081

7.3. Sensitivity study on thermal properties of gypsum board

This section presents a sensitivity study on the effect of the thermal properties of gypsum boards on the fire rating of the UL X530 assembly. The tested C-shaped column is 7 x 3 x 0.9'', with thickness of 0.066''. UL tested two configurations: one with 2 layers of ½'' Type C gypsum and one with 3 layers of ½'' Type C gypsum, as shown in Figure 22. During the tests, the columns were exposed to the ASTM E119 fire and temperatures were measured at different levels on the cross section [14].

(1) 1-hour rated assembly with 2 layers of ½'' Type C gypsum

(2) 2-hour rated assembly with 3 layers of ½'' Type C gypsum

Figure 22 Columns used in UL testing.

7.3.1. Data on thermal properties of Type X and Type C gypsum boards

The simulations in Section 7.2 adopted the gypsum board thermal properties from Cooper [12] for the Type X gypsum boards. In Section 7.3, thermal properties are required for Type C boards, since these were the ones used in the UL X530 fire tests.

There is a lack of guidance on thermal properties to adopt for different types of gypsum boards. Cooper does not specify what type of gypsum board the reported properties apply to. The properties are based on the research by Sultan [18], who tested Type X boards. However, Cooper's properties have been used for both Type X and Type C boards [22], with different values of density for either product (the higher density of the Type C boards resulting in higher insulation performance compared with Type X boards). Manzello et al. [20] concluded from his study that there is only minor difference in the thermal properties of Type X and Type C gypsum board.

Data from various researchers on the thermal properties of gypsum boards can be found in the literature [15–20]. Gypsum board from different sources or manufacturers varies in microstructure and methods employed to measure the thermal conductivity also differ, which results in variability in published data as shown in Figure 23. The test data by Mehaffey et al. agree well with those by Cooper [12] at temperature up to 400 °C (752 °F), beyond which the data by Mehaffey et al. [19] are lower than those by Cooper.

As for the specific heat, results from different studies are shown in Figure 24. These data agree well on the first peak, but there is certain discrepancy in terms of the temperature at which the second peak takes place as well as the values of the peaks. The data collected from the literature are summarized in Appendix F.

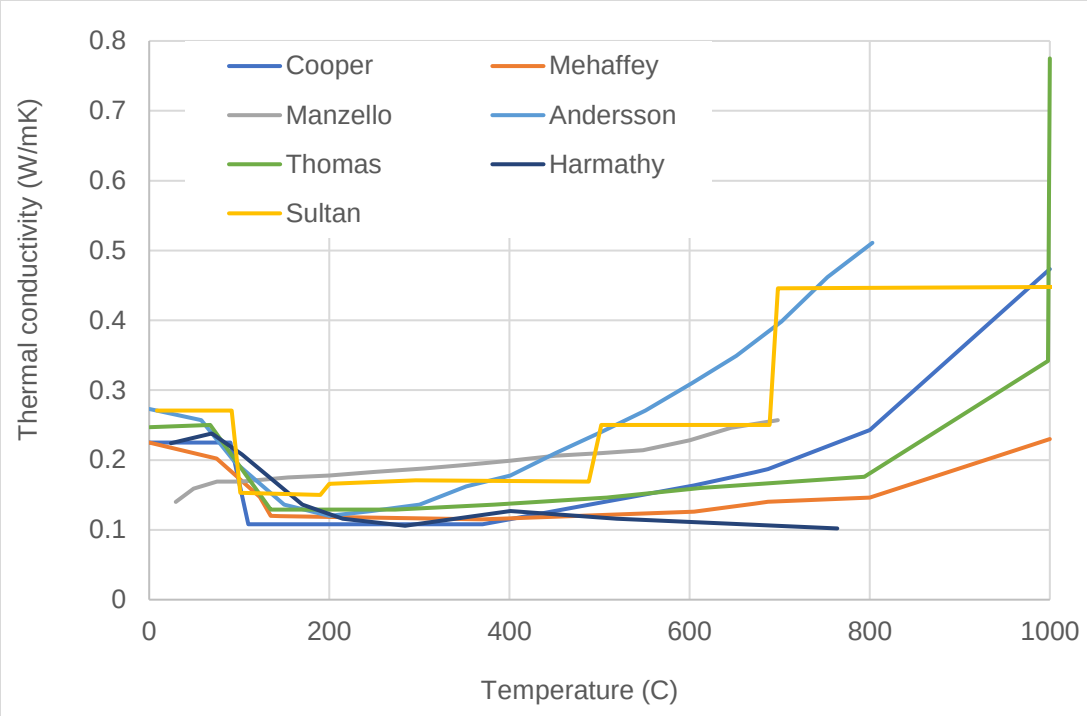

Figure 23 Thermal conductivity of Type X and Type C gypsum boards given by various tests.

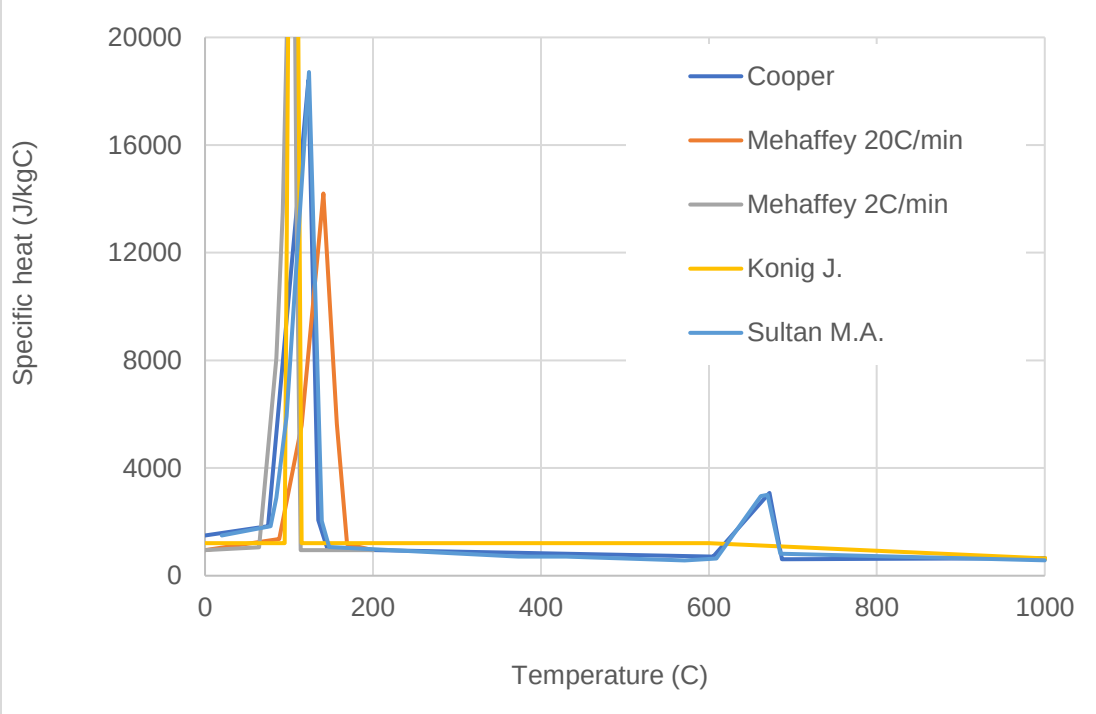

Figure 24 Specific heat of Type X and Type C gypsum boards given by various tests.

7.3.2. Comparison of numerical results with test data

To investigate the influence of thermal conductivity of gypsum board on member temperature, thermal analyses are performed on the UL X530 assembly with Type C gypsum board using the thermal conductivity data proposed by Cooper and that by Mehaffey. The member temperatures obtained with the two thermal conductivity models are compared with the UL test data [14] in Figure 25 and Figure 26 for the 1-hour rated and 2-hour rated assemblies, respectively.

The Cooper thermal conductivity data yields temperatures in the columns that substantially exceed the limiting temperature (1,000 °F) for both ratings (i.e., at 60 minutes with 2 layers of ½'' Type C gypsum board and at 120 minutes with 3 layers of ½'' Type C gypsum board). This suggests that the thermal conductivity data provided by Cooper is not applicable to Type C gypsum boards, or at least not to the ones used during the UL X530 fire tests.

When using the Mehaffey input data for thermal conductivity, the temperature in the 1-hour rated column remains below the limiting temperature. However, the temperature in the 2-hour rated column (with 3 layers of ½'' Type C gypsum board) exceeds the limiting temperature by about 10%. Even though the model by Mehaffey does not achieve the thermal requirement for 2-hour rated assembly, the results show the significant influence of the thermal conductivity input for the gypsum board on the member temperature.

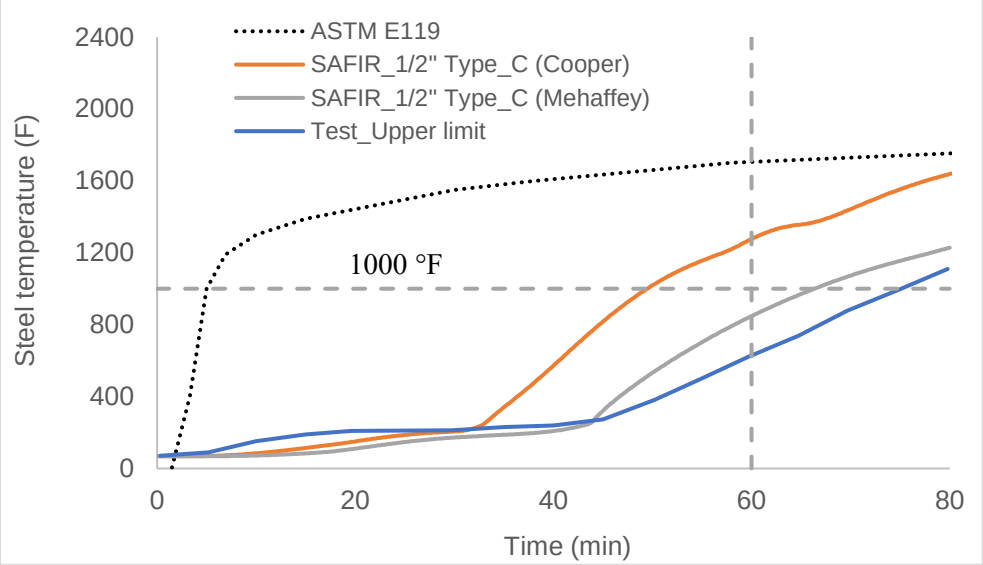

Figure 25 Evolution of steel temperature using different gypsum board thermal conductivity (1-hour rated assembly).

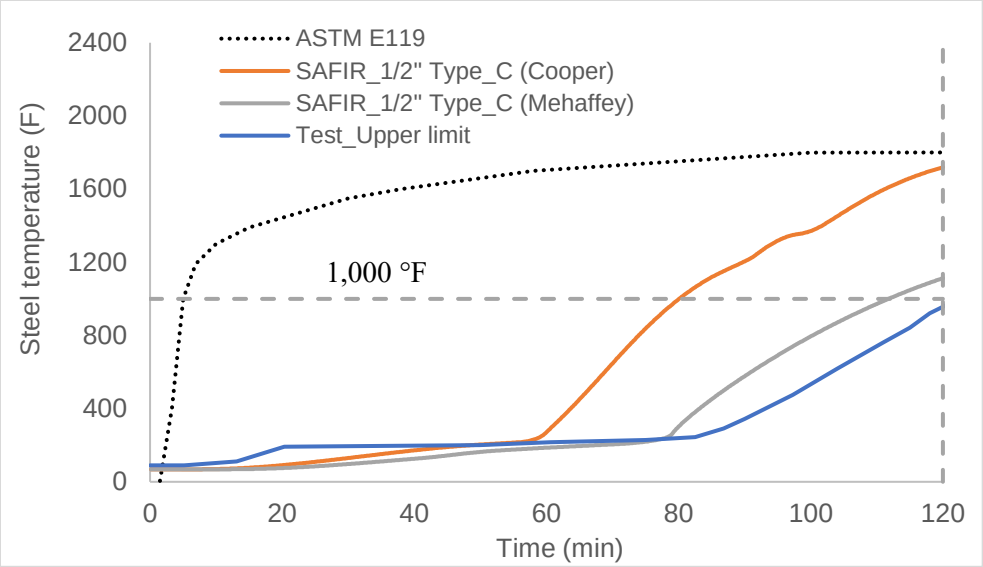

Figure 26 Evolution of steel temperature using different gypsum board thermal conductivity (2-hour rated assembly).

8. Conclusions

This report described the analysis of the fire performance of a metal building conducted according to the method of design by analysis in the newly proposed Appendix 4 to AISI S100 on 'Structural design for fire condition'. A prototype one-story warehouse metal building was adopted for the case study. The study focused on the load-bearing cold-formed steel column assemblies that were parts of the two end walls of the building. The assessment of the performance of the column assemblies under elevated temperatures due to fire conditions was presented step-by-step to illustrate the application of the proposed Appendix, including the definition of performance objectives, design-basis fires, thermal analysis, and structural strength analysis at an elevated temperature.

Considering the occupancy and size of the building, the required performance for the columns of the end walls was to maintain stability for one hour in case of an uncontrolled fire inside the warehouse. The columns were C-shaped cold-formed steel sections protected by gypsum board based on the UL X530 1-hour fire-resistance-rated assembly. In addition to the ASTM E119 standard fire curve, a set of design-basis fires generated with the fire zone modeling software OZone were considered. Thermal analyses of the columns subjected to the fires were conducted with the finite element software SAFIR. The failure time and failure temperature of each column was evaluated using both the AISI S100 Direct Strength Method (DSM) and finite element (FE) analysis. The analyses demonstrated satisfactory performance of the cold-formed steel assemblies, i.e., the columns maintain stability for over one hour of fire exposure. Specifically, the following conclusions can be drawn:

(1) Design-basis fires derived from physically-based zone models that consider the fuel, openings, geometry and properties of the compartment may result in sustained, severe thermal exposure conditions in a warehouse containing a large amount of fuel. The fuel load influences the fire duration while the ventilation conditions influence the peak gas temperatures. However, as the performance objective herein focuses on the first 60 minutes, the standard ASTM E119 fire results in more severe thermal exposure than the design-basis fires for this case study. This is mainly because the ASTM E119 time-temperature curve exhibits a very fast heating rate from the start. Therefore, consideration of the standard ASTM E119 time-temperature curve was conservative for this project.

(2) The heat transfer analysis of the protected cold-formed steel columns subjected to ASTM E119 fire led to steel temperatures ranging from 600-930 °F (315-500 °C) after 60 minutes. These results are consistent with the expected performance of the UL X530 1-hour fire resistance rated assembly used for the columns.

(3) The steel temperature was approximately uniform in the C-shaped columns heated on four faces. Therefore, the strength at elevated temperature could be assessed using AISI S100 with appropriately reduced steel mechanical properties. Elevated temperature properties provided in the newly proposed Appendix to AISI S100 were used herein.

(4) Application of AISI S100 showed that the strength of the columns after 60 minutes of ASTM E119 fire exposure remains larger than the applied forces resulting from the ASCE 7 load combination for the fire situation. The verification can also be made in the time domain by evaluating the failure time for each column; the failure time ranged between 100 minutes and 127 minutes.

(5) Finite element analysis with shell elements confirmed the results from AISI S100 and the proposed appendix. The failure time and failure temperature obtained with the two methods are close. Both methods demonstrate that the required performance is achieved for the end wall columns.

(6) For this prototype building, the analysis shows that the end wall columns with the UL X530 1-hour fire rating protection could maintain loadbearing stability for significantly longer than 1 hour of ASTM E119 fire exposure. This is because the required strength of the columns determined from the load combination in ASCE/SEI 7 for extraordinary events is much lower than the available strength for these columns for which the design at ambient temperature is governed by wind loads. As a result of the relatively low load ratio in the fire situation, the failure temperature of the columns is larger than the standard limiting steel temperature used in furnace testing. This eventually results in a longer duration of stability. This study thus demonstrates that the fire resistance depends on the applied loading. Most standard fire resistance rated column assemblies have been developed from unloaded test specimens and based on the limiting steel temperatures specified in ASTM E119. Other types of wall, floor, roof and beam assemblies are usually tested with maximum design loads. Therefore, for elements and structures which are lightly loaded in the fire situation, analysis methods can be used to demonstrate superior performance compared to a given fire resistance rating.

(7) Thermal analyses of fire-rated assemblies show the important influence of the assumed thermal properties of gypsum on the computed temperatures in the steel. Yet, data from the literature reveal significant variability in thermal conductivity of gypsum, and there is a lack of guidance in standard documents. To support the development of analysis methods for cold-formed steel assemblies, it is recommended that future studies focus on the issue of thermal properties of the fire protection materials at elevated temperature.

(8) The study analyzed a double C-shaped assembly (EC-3 and E-C8) for which no standard fire resistance rating exists. It was shown through FE thermal analysis that the double C-shaped assembly can achieve a 1-hour fire rating based on the ASTM E119 limiting temperature criteria with 2 layers of 5/8'' Type X gypsum boards assembled according to the UL X530 assembly. The analysis suggests that the assembly could also pass the test using 2 layers of 1/2'' Type X gypsum assembled according to the UL X530 assembly. Indeed, the temperature increase in the double C-shaped member is slower than that in the equivalent single C-shaped member owing to the favorable section factor of the former as compared with the latter. This example illustrates how the analysis methods can be used to study variations of qualified assemblies to determine appropriate adjustments in fire protection.

(9) The study analyzed single C-shaped assemblies (EC-2 and EC-4) with fire protection configuration modified from the qualified assembly UL X530. It was shown that the modified assemblies, which differ from the qualified UL X530 by the layout of the gypsum boards, have similar performance as the UL X530 assembly. Specifically, they can achieve a 1-hour fire rating based on the ASTM E119 limiting temperature criteria with 2 layers of 5/8'' Type X gypsum boards.

Appendix A. Temperature distribution of columns at 60 minutes of fire exposure

Note: thermal analyses in this appendix are conducted using the thermal properties of gypsum board from Cooper [12], as provided in Figure 14.

Temperature distributions given at 60 minutes of exposure to ASTM E119 and design-basis fires.

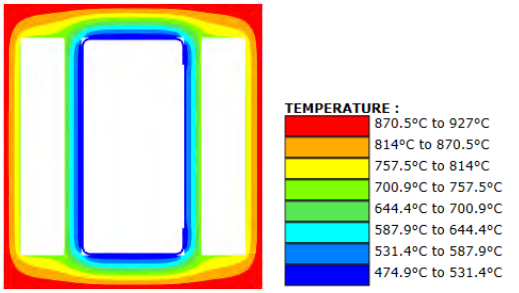

(1) EC-1/EC-5

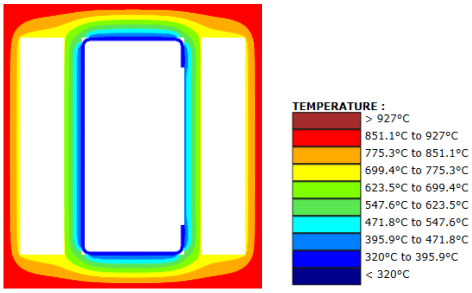

(2) EC-2

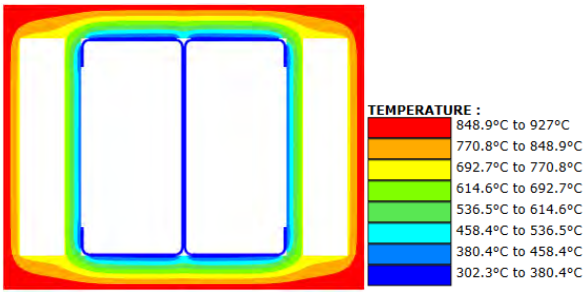

(3) EC-3

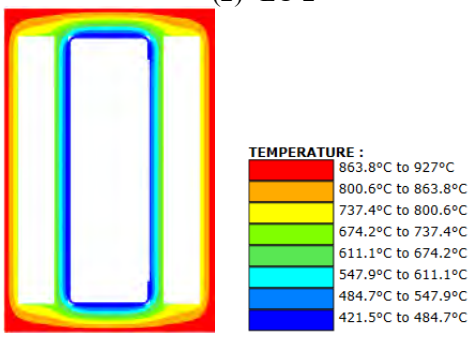

(4) EC-4

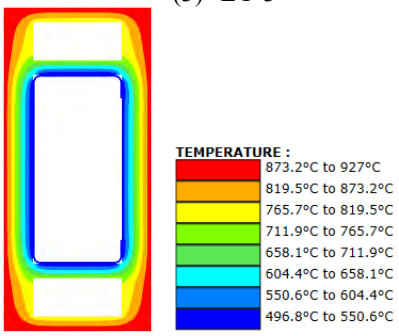

(5) EC-6/EC-10

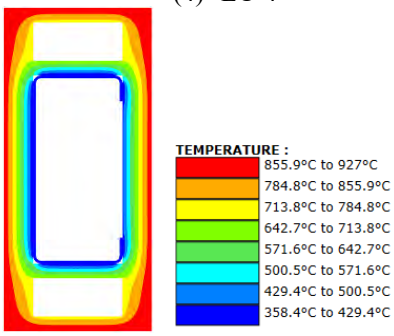

(6) EC-7

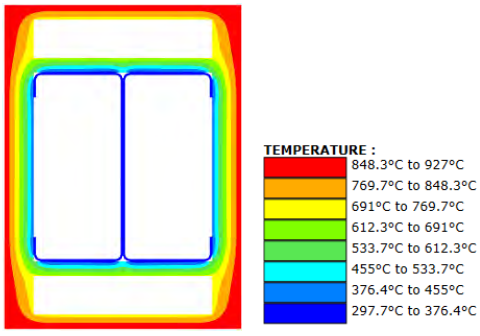

(7) EC-8

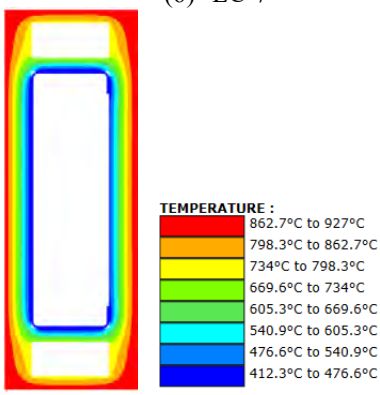

(8) EC-9

Figure 27 Temperature distribution of columns at 60 minutes under ASTM E119 fire.

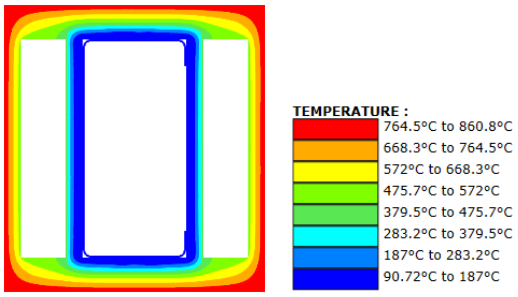

(1) EC-1/EC-5

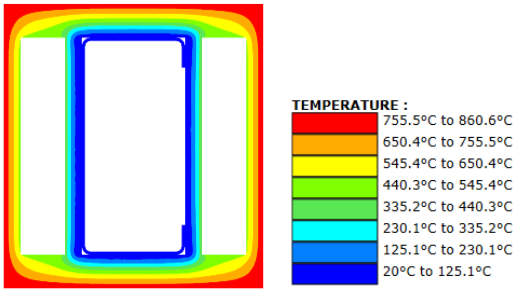

(2) EC-2

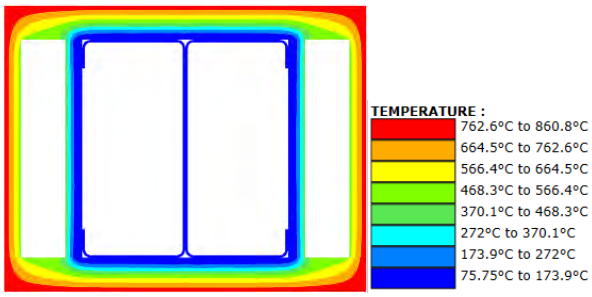

(3) EC-3

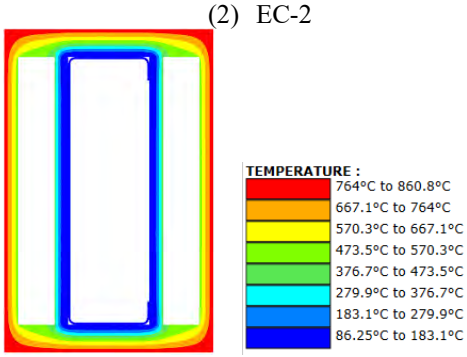

(4) EC-4

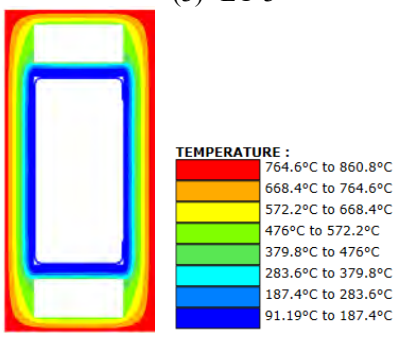

(5) EC-6/EC-10

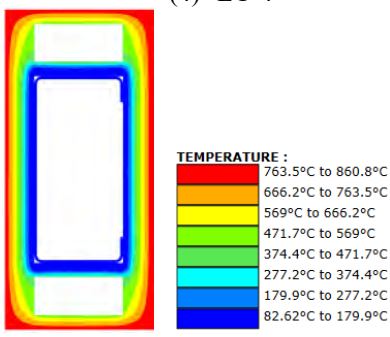

(6) EC-7

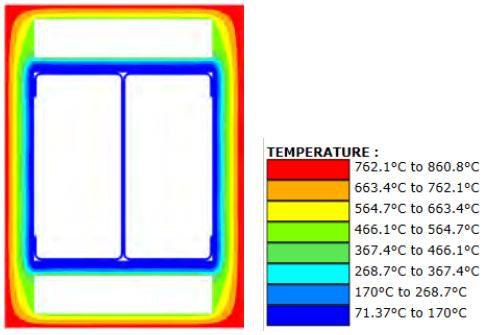

(7) EC-8

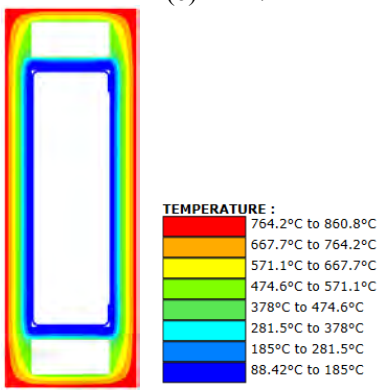

(8) EC-9

Figure 28 Temperature distribution of column at 60 minutes under OZone fire_Entire floor_50%.

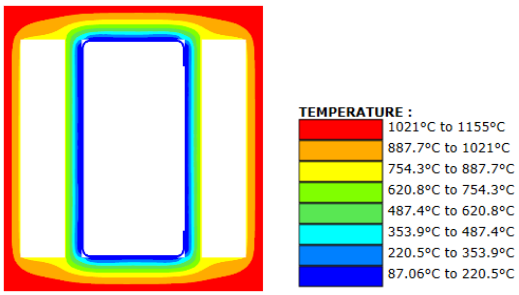

(1) EC-1/EC-5

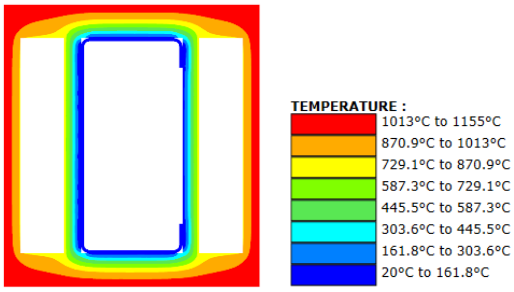

(2) EC-2

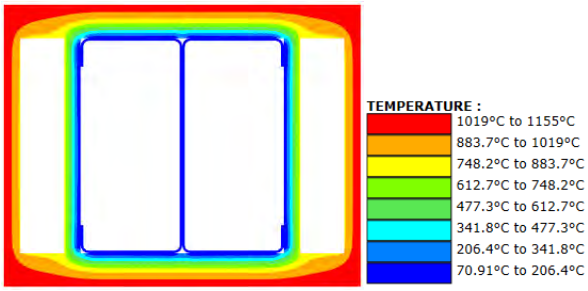

(3) EC-3

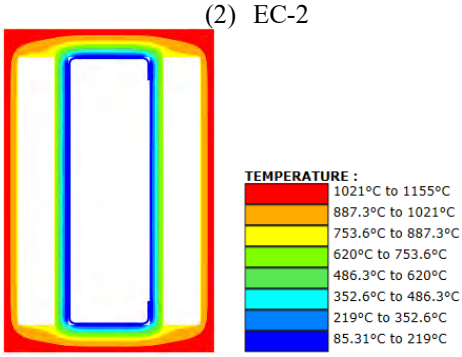

(4) EC-4

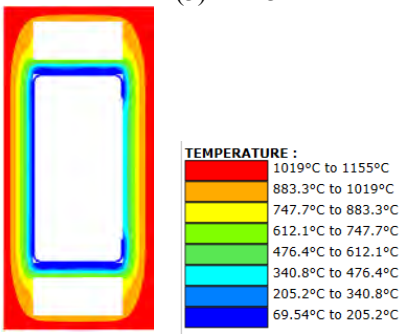

(5) EC-6/EC-10

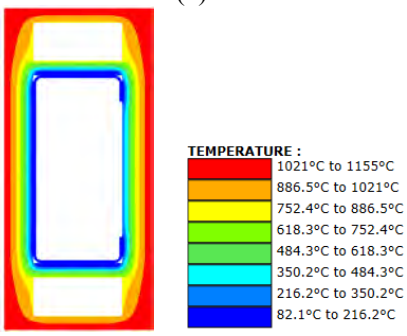

(6) EC-7

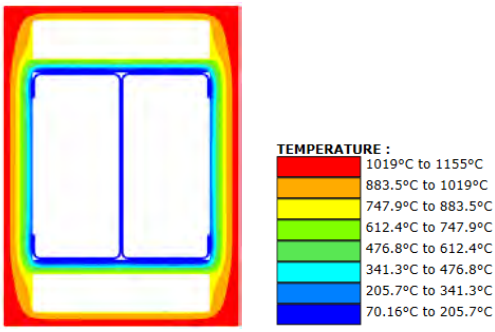

(7) EC-8

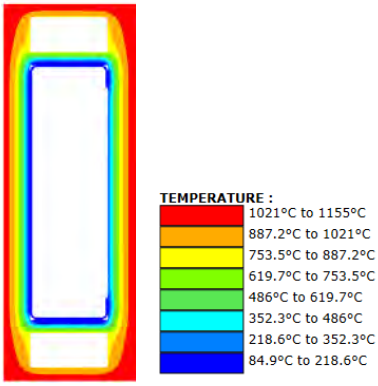

(8) EC-9

Figure 29 Temperature distribution of column at 60 minutes under OZone fire_Entire floor_100%.

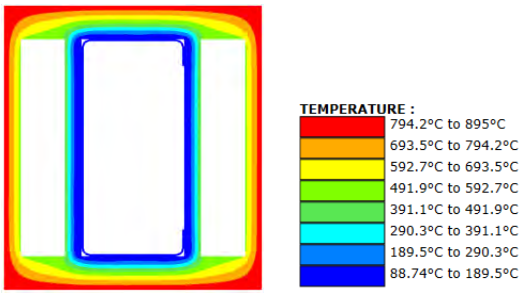

(1) EC-1/EC-5

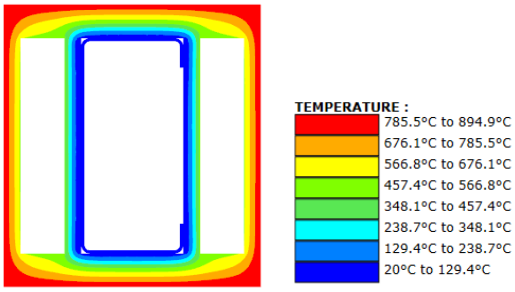

(2) EC-2

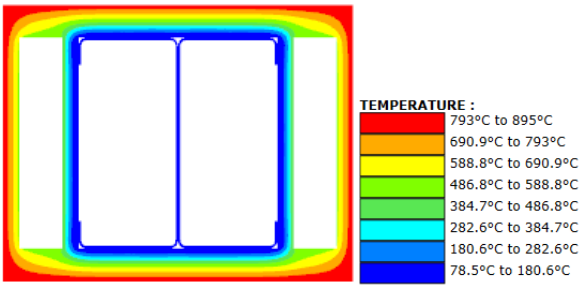

(3) EC-3

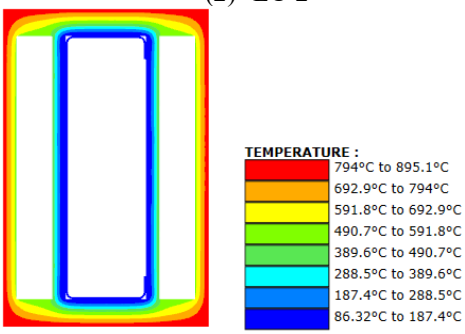

(4) EC-4

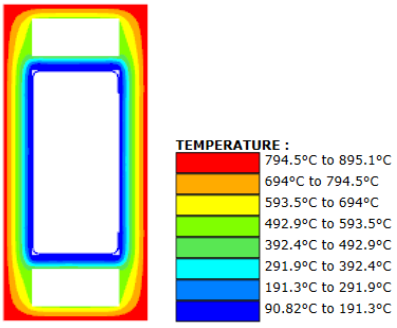

(5) EC-6/EC-10

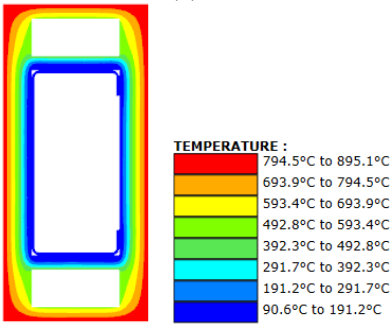

(6) EC-7

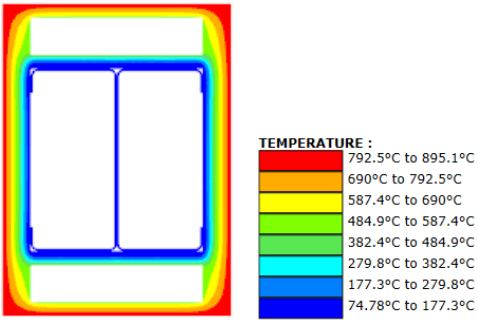

(7) EC-8

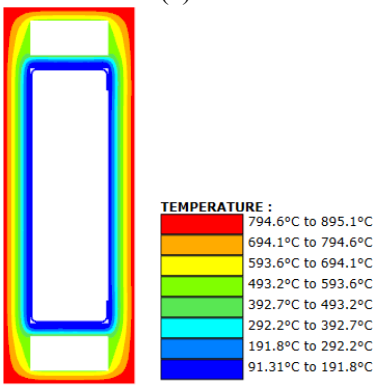

(8) EC-9

Figure 30 Temperature distribution of each column at 60 minutes under OZone fire_ Warehouse area _50%.

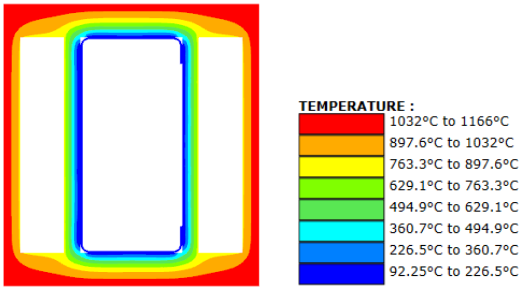

(1) EC-1/EC-5

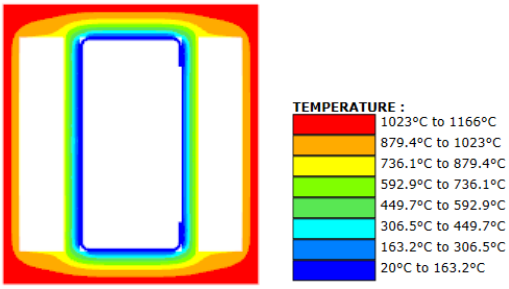

(2) EC-2

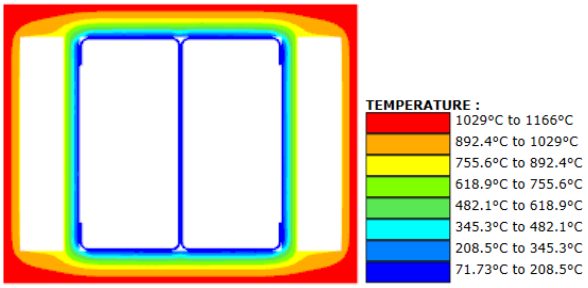

(3) EC-3

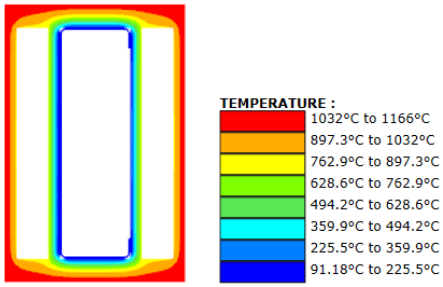

(4) EC-4

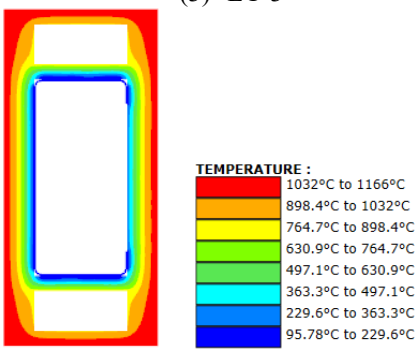

(5) EC-6/EC-10

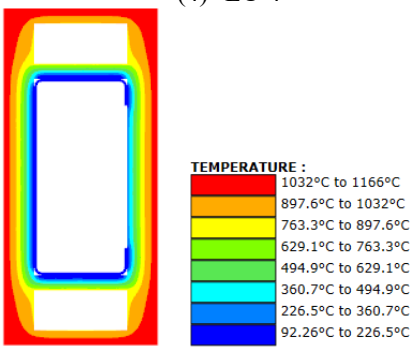

(6) EC-7

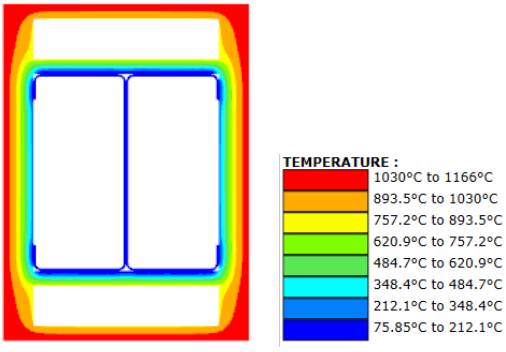

(7) EC-8

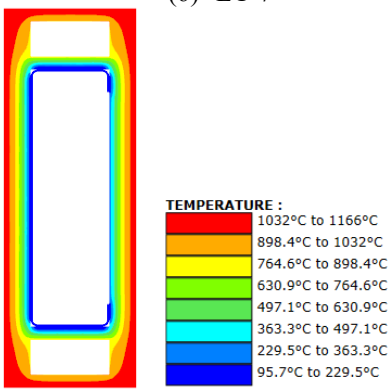

(8) EC-9

Figure 31 Temperature distribution of each column at 60 minutes under OZone fire_ Warehouse area _100%.

Appendix B. Steel properties at elevated temperature

The proposed Fire Appendix to AISI S100 [1] specifies that mechanical properties for elastic modulus E, shear modulus G, yield stress F_y, and tensile stress F_u of cold-formed steels at elevated temperature can be obtained by multiplying the ambient temperature properties by reduction (retention) factors k_E, k_G, k_y, k_u, respectively. The reduction factors should be taken as follows:

$$k_E, k_G, k_y, k_u = (1-c)\frac{1-x^b}{1+ax^b} + c$$

where $x = \frac{T-T_1}{T_2-T_1}$, T is the steel temperature, $T_1 = 68$ °F (20 °C), $T_2 = 1832$ °F (1000 °C), a, b, c are defined in the following table. Background for the derivation of these equations is given in Xia et al. [21].

Table 20 Coefficients for reduction factors of steel mechanical properties.

Reduction factor	a	b	c
k_E, k_G	8	3	0.04
k_y	20	4	0.03
k_u	185	7	0.04

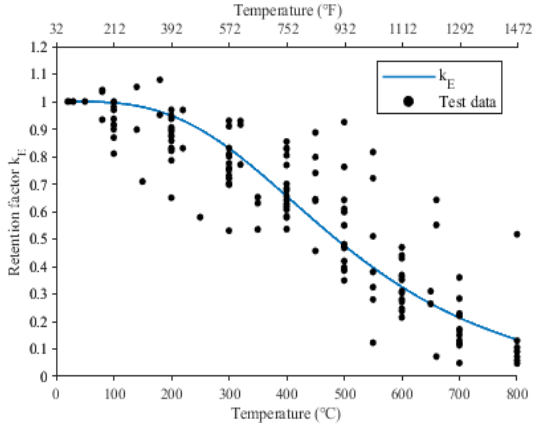

(1) k_E, k_G

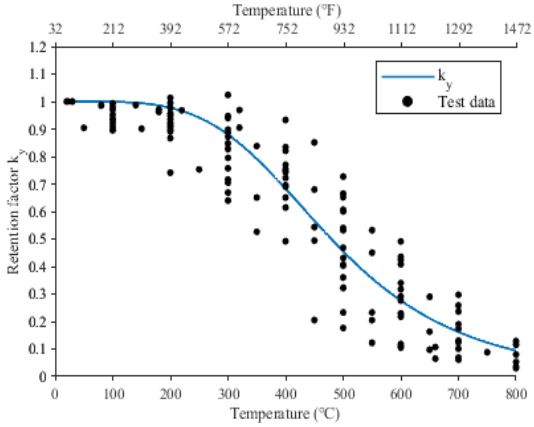

(2) k_y

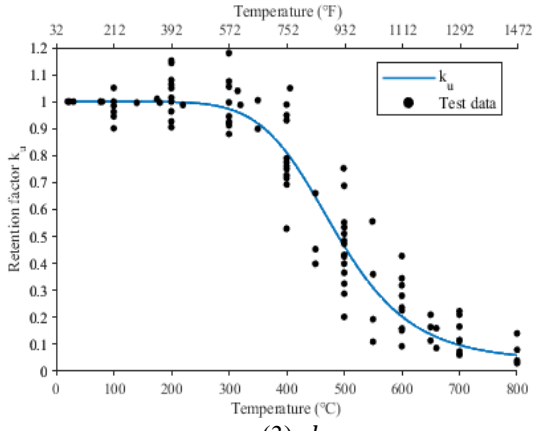

(3) k_u

Figure 32 Retention factors for steel mechanical properties.

Appendix C. Worked example on EC-6 (1 hr. rated assembly)

Nomenclature

A_f	Cross-sectional area of flange	K_x	Effective length factor for bending about x-axis
A_g	Gross cross-sectional area	K_y	Effective length factor for bending about y-axis
b	Flange length (mid-line dimension)	K_t	Effective length factor for twisting
C_w	Torsional warping constant of cross-section	L	Min (L_{crd}, L_m)
C_{wf}	Warping torsion constant of flange	L_{crd}	Critical unbraced length of distortional buckling
d	Length of the lip (mid-line dimension)	L_m	Distance between discrete restraints that restrict distortional buckling (for continuously restrained members L_m =L_{crd})
E	Modulus of elasticity of steel	L_x	Unbraced length of member for bending about x-axis
F_{cre}	Critical global buckling stress	L_y	Unbraced length of member for bending about y-axis
F_{crl}	Smallest local buckling stress of all elements in cross-section	L_t	Unbraced length of member for torsion
F_y	Yield stress	P_{crd}	Critical elastic distortional column buckling strength
G	Shear modulus of steel	P_{crl}	Critical elastic local column buckling load
h	Height of the cross section (mid-line dimension)	P_{nd}	Distortional buckling strength
h_o	Web depth (mid-line dimension)	P_{ne}	Global buckling strength
h_{xf}	x distance from centroid of flange to flange/web junction	P_{nl}	Local buckling strength
h_{xyf}	y distance from centroid of flange to flange/web junction	r_o	Polar radius of gyration about shear center = $\sqrt{x_0^2 + y_0^2 + r_x^2 + r_y^2}$
I_{xf}	x-axis moment of inertia of flange	r_x	Radius of gyration of full unreduced cross-section about x-axis
I_{yf}	y-axis moment of inertia of flange	r_y	Radius of gyration of full unreduced cross-section about y-axis
I_{xyf}	Product of the moment of inertia of flange	t	Thickness of cross section
J	St. Venant torsion constant of cross-section	w	Flat width of elements in the cross section
J_f	St. Venant torsion constant of flange	x_o	Distance from centroid to shear center in principal x-axis direction
k	Plate buckling coefficient	x_{of}	x distance from centroid of flange to shear center of flange
$k_{\phi fe}$	Elastic rotational stiffness provided by the flange to the flange/web juncture	y_o	Distance from centroid to shear center in principal y-axis direction
$k_{\phi we}$	Elastic rotational stiffness provided by the web to flange/web juncture	y_{of}	y distance from centroid of flange to shear center of flange
$k_{\phi fg}$	Geometric rotational stiffness demanded by flange from flange/web juncture	σ_{ex}	Elastic flexural buckling stress about principal x-axis
$k_{\phi wg}$	Geometric rotational stiffness demanded by web from flange/web juncture	σ_{ey}	Elastic flexural buckling stress about principal y-axis
k_ϕ	Rotational stiffness provided by restraining elements (brace, panel, sheathing) to flange/web juncture of member (zero if the flange is unrestrained)	σ_t	Torsional buckling stress

C.1. Member information

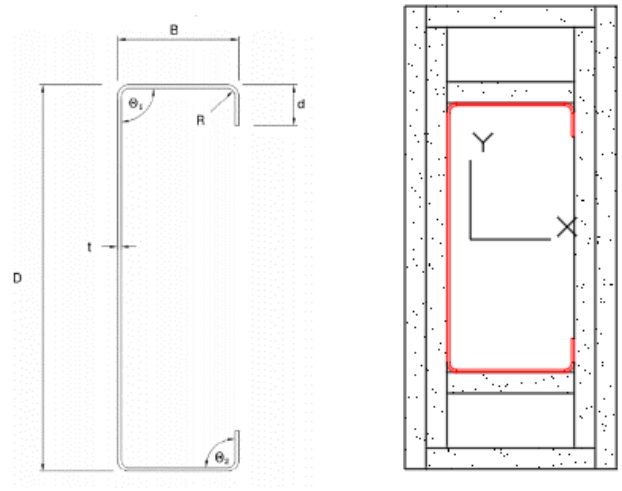

Figure 33 Dimension and fire protection assembly for column EC-6. (enclosed within two layers of 5/8-inch Type X gypsum board)

Table 21 Dimensions of EC-6.

Column	Grade (ksi)	Part	D (in.)	B (in.)	R (in.)	d (in.)	t (in.)
EC-6	55	W08S075	8	3.78	0.25	0.992	0.075

Table 22 Unbraced length of EC-6.

Column	Unbraced length	
	Major axis, x (ft.)	Minor axis, y (ft.)
EC-6	18.4	7.5

C.2. Applied loading during fire

Table 23 Forces in column EC-6 in the fire situation.

Column	Axial force (k)	Shear force (k)	Moment (f-k)
EC-6	0.9	0	0

C.3. Performance objective

The cold-formed steel column is required to maintain its load-bearing function during 1 hour of standard fire exposure on 4 sides.

C.4. Thermal analysis

The heat transfer analysis is carried out by finite element simulation. The software SAFIR is used. The thermal properties for steel are taken from the proposed AISI Fire Appendix. The thermal properties for gypsum are taken from Cooper [12]. The emissivity is taken as 0.7 and the convection heat transfer coefficient is 25 W/m^2k (4.4 $Btu/(hr \cdot ft^2 \cdot °F)$).

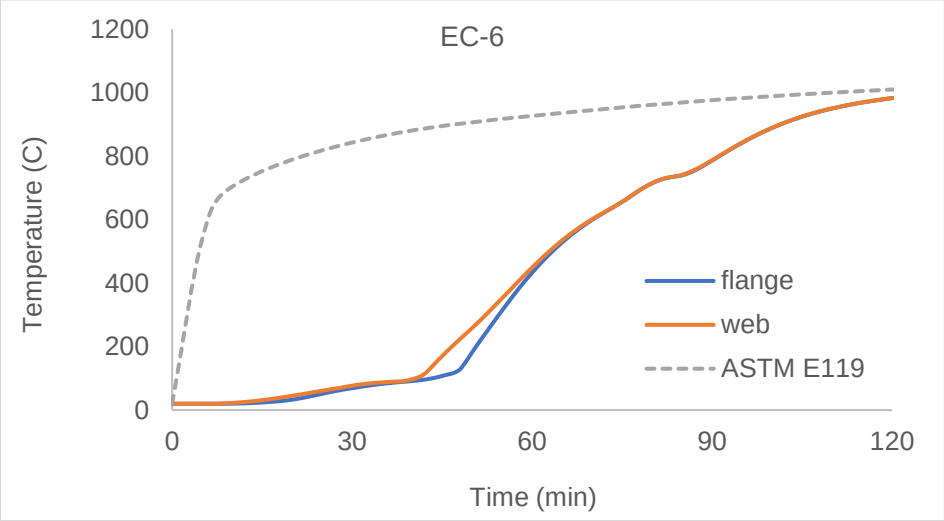

Figure 34 Temperature history at the flange and web of EC-6.

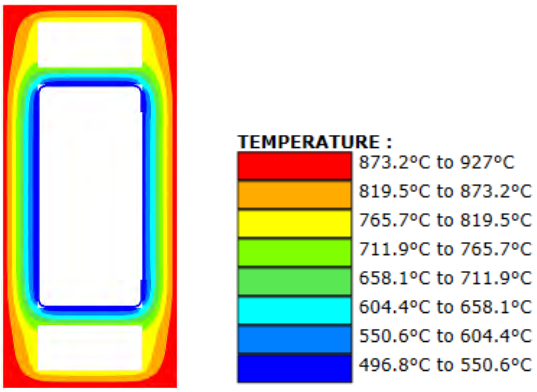

Figure 35 Temperature distribution at 60 min under ASTM E119 fire.

C.5. Nominal Strength at ambient temperature

C.5.1. AISI S100 DSM

(4) Global buckling strength

The global buckling strength is calculated with the following equations.

$$P_{ne} = AF_n$$

$$F_n = \begin{cases} 0.658^{\lambda_c^2} F_y & for\ \lambda_c \leq 1.5 \\ \dfrac{0.877}{\lambda_c^2} F_y & for\ \lambda_c > 1.5 \end{cases}$$

where A is the gross area, F_n is the compressive stress, $\lambda_c = \sqrt{\frac{F_y}{F_{cre}}}$, and F_{cre} is the least of the applicable elastic global (flexural, torsional, and flexural-torsional) buckling stresses.

Cross-section properties

The cross-section properties are calculated from the open-source program CUFSM [23].

$A = 1.26\ in^2$	$I_x = 13.1\ in^4$	$I_y = 2.49\ in^4$
$J = 0.00236\ in^4$	$C_w = 33.2\ in^6$	$x_0 = -2.97\ in$
$r_x = 3.22\ in$	$r_y = 1.41\ in$	$r_0 = 4.60\ in$

Length and bracing conditions

$K_x = 1$	$K_y = 1$	$K_t = 1$
$L_x = 90\ in$	$L_y = 220.8\ in$	$L_t = 90\ in$

Retention factors (ambient)

$T = 68$ °F	$k_E = 1.00$	$k_y = 1.00$
$E = 29500\ ksi$	$F_y = 55\ ksi$	$G = 11346\ ks$

Individual buckling modes

$\sigma_{ex} = 61.8\ ksi$	$\sigma_{ey} = 71.1\ ksi$	$\sigma_t = 45.7\ ksi$

Torsional-flexural buckling

F_{cre} is determined as the smallest root of the following equation:

$$(F_{cre} - \sigma_{ex})(F_{cre} - \sigma_{ey})(F_{cre} - \sigma_t) - F_{cre}^2(F_{cre} - \sigma_{ey})\left(\frac{x_0}{r_0}\right)^2 - F_{cre}^2(F_{cre} - \sigma_{ey})\left(\frac{y_0}{r_0}\right)^2 = 0$$

$F_{cre} = 31.7\ ksi$

$\lambda_c = \sqrt{\frac{F_y}{F_{cre}}} = 1.32 < 1.5$

$F_n = 0.658^{\lambda_c^2} F_y = 26.6\ ksi$

The global buckling strength is: $P_{ne} = AF_n = 33.6\ kip$

(5) Local buckling strength

The local buckling strength is calculated with the following equations.

$$P_{nl} = \begin{cases} P_{ne} & for\ \lambda_l \le 0.776 \\ \left[1 - 0.15\left(\frac{P_{crl}}{P_{ne}}\right)^{0.4}\right]\left(\frac{P_{crl}}{P_{ne}}\right)^{0.4} P_{ne} & for\ \lambda_l > 0.776 \end{cases}$$

where $\lambda_l = \sqrt{\frac{P_{ne}}{P_{crl}}}$, P_{ne} is the global buckling strength, P_{crl} is the critical elastic local column buckling load calculated as follows:

$$P_{crl} = AF_{crl}$$

where A is the gross area, F_{crl} is the smallest local buckling stress of all elements in cross-section.

$$F_{crl} = k\frac{\pi^2 E}{12(1-\mu^2)}\left(\frac{t}{w}\right)^2$$

Web local buckling

$k = 4$ $t = 0.075\ in$ $w = 7.43\ in$

$F_{crl\_web} = 10.9\ ksi$

Flange local buckling

$k = 4$ $t = 0.075\ in$ $w = 3.21\ in$

$F_{crl\_flange} = 58.3\ ksi$

Lip local buckling

$k = 0.43$ $t = 0.075\ in$ $w = 0.705\ in$

$F_{crl\_lip} = 129.8\ ksi$

$F_{crl} = \min(F_{crl_{web}} \quad F_{crl_{flange}} \quad F_{crl_{lip}}) = 10.9\ ksi$

$P_{crl} = AF_{crl} = 13.7\ kip$

$$\lambda_l = \sqrt{\frac{P_{ne}}{P_{crl}}} = 1.57 > 0.776$$

$$P_{nl} = \left[1 - 0.15\left(\frac{P_{crl}}{P_{ne}}\right)^{0.4}\right]\left(\frac{P_{crl}}{P_{ne}}\right)^{0.4} P_{ne} = 21.0\ kip$$

(6) Distortional buckling strength

The distortional buckling strength is calculated with the following equations.

$$P_{nd} = \begin{cases} P_y \quad for\ \lambda_d \le 0.561 \\ \left[1 - 0.25\left(\frac{P_{crd}}{P_y}\right)^{0.6}\right]\left(\frac{P_{crd}}{P_y}\right)^{0.6} P_y \quad for\ \lambda_d > 0.561 \end{cases}$$

where $\lambda_d = \sqrt{\frac{P_y}{P_{crd}}}$, $P_y = AF_y$, P_{crd} is the Critical elastic distortional column buckling load calculated as follows.

$$P_{crd} = AF_{crd}$$

Mid-line dimensions of cross-section

$b = 3.71\ in$	$d = 0.955\ in$	$h = 7.93\ in$
$t = 0.075\ in$	$h_o = 8.00\ in$	

Cross-section properties

The cross-section properties are calculated from the open-source program CUFSM [23].

$A_f = 0.349\ in^2$	$J_f = 0.000655\ in^4$	$I_{xf} = 0.0185\ in^4$
$I_{yf} = 0.513\ in^4$	$I_{xyf} = 0.0503\ in^4$	$C_{wf} = 0.00\ in^2$
$x_{of} = 1.47\ in$	$y_{of} = -0.0978\ in$	$h_{xf} = -2.23\ in$
$h_{yf} = -0.0978\ in$		

F_{crd}

$L_{crd} = 37.0\ in$	$L_m = 37.0\ in$	$L = 37.0\ in$
$k_{\phi fe} = 0.338\ kip$	$k_{\phi we} = 0.285\ kip$	$k_{\phi fg} = 0.0169\ in^2$
$k_{\phi wg} = 0.00460\ in^2$	$k_\phi = 0$	$F_{crd} = 29.0\ ksi$

$$P_{crd} = AF_{crd} = 36.6\ kip$$

$$\lambda_d = \sqrt{\frac{P_y}{P_{crd}}} = 1.38 > 0.561$$

$$P_y = AF_y = 69.3\ kip$$

$$P_{nd} = \left[1 - 0.25\left(\frac{P_{crd}}{P_y}\right)^{0.6}\right]\left(\frac{P_{crd}}{P_y}\right)^{0.6} P_y = 39.2\ kip$$

(7) Nominal capacity at ambient temperature

$\lambda_c = 1.32$ $P_{ne} = 33.6\ kip$

$\lambda_l = 1.57$ $P_{nl} = 21.0\ kip$

$\lambda_d = 1.38$ $P_{nd} = 39.2\ kip$

$$P_{DSM} = \min(P_{ne}, P_{nl}, P_{nd}) = P_{nl} = 21.0\ kip$$

The controlling failure mode is local buckling.

C.5.2. FEM analysis

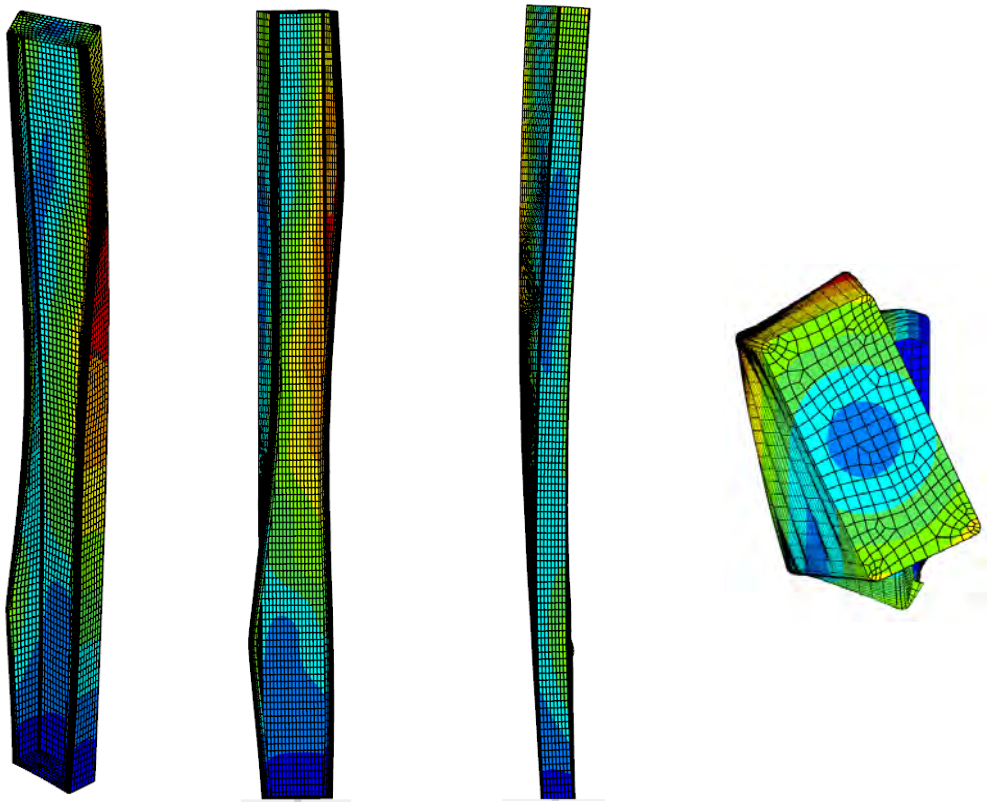

Figure 36 Failure mode at ambient temperature.

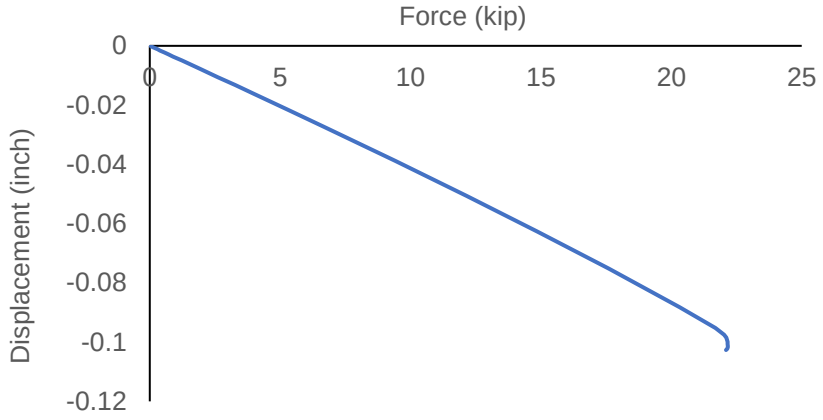

Figure 37 Force-displacement curve at ambient temperature.

Table 24 Capacity of column EC-6 at ambient temperature.

Columns	AISI S100 DSM Nominal Strength (kip)	SAFIR/Shell FE (kip)
EC-6	21.0	22.1

C.6. Nominal Strength at 60 minutes under ASTM E119 (AISI S100 DSM)

At 60 minutes, the steel temperature of EC-6 is 930 °F (499 °C). The reduction factors are taken at a temperature of 930 °F (499 °C).

(8) Global buckling strength

Retention factors

$T = 930$ °F $\quad k_E = 0.478 \quad k_y = 0.457$

$E, T = 14112\ ksi \quad F_y, T = 25.1\ ksi \quad G, T = 5428\ ksi$

Individual buckling modes

$\sigma_{ex} = 29.6\ ksi \quad \sigma_{ey} = 34.0\ ksi \quad \sigma_t = 21.9\ ksi$

Torsional-flexural buckling

$F_{cre} = 15.2\ ksi$

$$\lambda_c = \sqrt{\frac{F_{y,T}}{F_{cre}}} = 1.29 < 1.5$$

$F_n = 0.658^{\lambda_c^2} F_{y,T} = 12.6\ ksi$

The global buckling strength is: $P_{ne} = AF_n = 15.8\ kip$

(9) Local buckling strength

Web local buckling

$k = 4 \quad t = 0.075\ in \quad w = 7.43\ in$

$F_{crl\_web} = 5.20\ ksi$

Flange local buckling

$k = 4 \quad t = 0.075\ in \quad w = 3.21\ in$

$F_{crl\_flange} = 27.9\ ksi$

Lip local buckling

$k = 0.43 \quad t = 0.075\ in \quad w = 0.705\ in$

$F_{crl\_lip} = 62.1\ ksi$

$F_{crl} = \min (F_{crl_{web}} \quad F_{crl_{flange}} \quad F_{crl_{lip}}) = 5.20\ ksi$

$P_{crl} = AF_{crl} = 6.55\ kip$

$\lambda_l = \sqrt{\frac{P_{ne}}{P_{crl}}} = 1.55 > 0.776$

$P_{nl} = \left[1 - 0.15\left(\frac{P_{crl}}{P_{ne}}\right)^{0.4}\right]\left(\frac{P_{crl}}{P_{ne}}\right)^{0.4} P_{ne} = 10.0\ kip$

(10) Distortional buckling strength

$\boldsymbol{F_{crd}}$

$L_{crd} = 37.0\ in$	$L_m = 37.0\ in$	$L = 37.0\ in$
$k_{\phi fe} = 0.162\ kip$	$k_{\phi we} = 0.136\ kip$	$k_{\phi fg} = 0.0169\ in^2$
$k_{\phi wg} = 0.00460\ in^2$	$k_{\phi} = 0$	$F_{crd} = 13.9\ ksi$

$P_{crd} = AF_{crd} = 17.5\ kip$

$\lambda_d = \sqrt{\frac{P_y}{P_{crd}}} = 1.35 > 0.561$

$P_y = AF_{y,T} = 31.7\ kip$

$P_{nd} = \left[1 - 0.25\left(\frac{P_{crd}}{P_y}\right)^{0.6}\right]\left(\frac{P_{crd}}{P_y}\right)^{0.6} P_y = 18.3\ kip$

(11) Nominal capacity at 60 minutes under ASTM E119

$\lambda_c = 1.29$	$P_{ne} = 15.8\ kip$
$\lambda_l = 1.55$	$P_{nl} = 10.0\ kip$
$\lambda_d = 1.35$	$P_{nd} = 18.3\ kip$

$P_{DSM} = \min(P_{ne}, P_{nl}, P_{nd}) = P_{nl} = 10.0\ kip$

The controlling failure mode is local buckling.

C.7. Failure temperature and failure time

C.7.1. AISI S100 DSM

The AISI S100 DSM is applied iteratively to find the temperature at which the nominal strength equals the required strength. After iterations, the failure temperature is 981 °C (1,798 °F). Details of the calculation at 1,798 °F are given below.

(12) Global buckling strength

Retention factors

$T = 1798\ °\text{F}$ $k_E = 0.046$ $k_y = 0.034$

$E, T = 1369\ ksi$ $F_y, T = 1.86\ ksi$ $G, T = 527\ ksi$

Individual buckling modes

$\sigma_{ex} = 2.87\ ksi$ $\sigma_{ey} = 3.30\ ksi$ $\sigma_t = 2.12\ ksi$

Torsional-flexural buckling

$F_{cre} = 1.47\ ksi$

$$\lambda_c = \sqrt{\frac{F_{y,T}}{F_{cre}}} = 1.12 < 1.5$$

$F_n = 0.658^{\lambda_c^2} F_{y,T} = 1.10\ ksi$

The global buckling strength is: $P_{ne} = AF_n = 1.38\ kip$

(13) Local buckling strength

Web local buckling

$k = 4$ $t = 0.075\ in$ $w = 7.43\ in$

$F_{crl\_web} = 0.504\ ksi$

Flange local buckling

$k = 4$ $t = 0.075\ in$ $w = 3.21\ in$

$F_{crl\_flange} = 2.71\ ksi$

Lip local buckling

$k = 0.43$ $t = 0.075\ in$ $w = 0.705\ in$

$F_{crl\_lip} = 6.02\ ksi$

$F_{crl} = \min(F_{crl_{web}} \quad F_{crl_{flange}} \quad F_{crl_{lip}}) = 0.504\ ksi$

$P_{crl} = AF_{crl} = 0.636\ kip$

$\lambda_l = \sqrt{\frac{P_{ne}}{P_{crl}}} = 1.47 > 0.776$

$P_{nl} = \left[1 - 0.15\left(\frac{P_{crl}}{P_{ne}}\right)^{0.4}\right]\left(\frac{P_{crl}}{P_{ne}}\right)^{0.4} P_{ne} = 0.901\ kip$

(14) Distortional buckling strength

$\boldsymbol{F_{crd}}$

$L_{crd} = 37.0\ in$	$L_m = 37.0\ in$	$L = 37.0\ in$
$k_{\phi fe} = 0.0157\ kip$	$k_{\phi we} = 0.0132\ kip$	$k_{\phi fg} = 0.0169\ in^2$
$k_{\phi wg} = 0.00460\ in^2$	$k_{\phi} = 0$	$F_{crd} = 1.35\ ksi$

$P_{crd} = AF_{crd} = 1.70\ kip$

$\lambda_d = \sqrt{\frac{P_y}{P_{crd}}} = 1.17 > 0.561$

$P_y = AF_{y,T} = 2.34\ kip$

$P_{nd} = \left[1 - 0.25\left(\frac{P_{crd}}{P_y}\right)^{0.6}\right]\left(\frac{P_{crd}}{P_y}\right)^{0.6} P_y = 1.53\ kip$

(15) Nominal capacity at temperature of 981 °C (1798 °F)

$\lambda_c = 1.12$	$P_{ne} = 1.38\ kip$
$\lambda_l = 1.47$	$P_{nl} = 0.901\ kip$
$\lambda_d = 1.17$	$P_{nd} = 1.53\ kip$

$P_{DSM} = \min(P_{ne}, P_{nl}, P_{nd}) = P_{nl} = 0.901\ kip$

The controlling failure mode is local buckling.

$P_{DSM} = 0.901\ kip \approx F = 0.9\ kip$

Utilization ratio = $\frac{P_{DSM}}{F} = 1.00$

From thermal analysis: $T_f = 981℃\ @\ t = 116\ min$

C.7.2. FEM analysis

A transient FE analysis was run. The simulation stopped when the member temperature reached 1000 °C (1,832 °F), which is the upper limit of applicability of the steel mechanical property models in AISI S100. Failure had not yet been reached.

Table 25 Failure time and failure temperature under ASTM E119 fire.

Columns	DSM		SAFIR/Shell FE	
	Failure time (min)	Failure temperature (°F/°C)	Failure time (min)	Failure temperature (°F/°C)
EC-6	116	1798 / 981	120+	1832+ / 1000+

Appendix D. Worked example on EC-8 (1 hr. rated assembly)

D.1. Member information

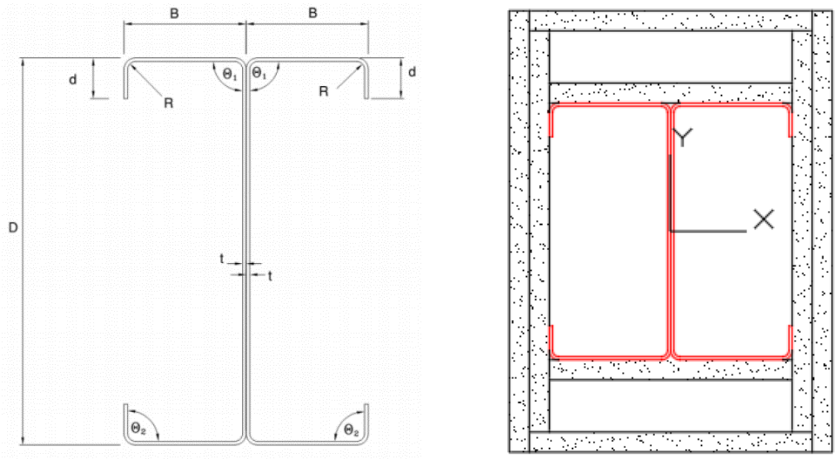

Figure 38 Dimension and fire protection configuration of EC-8. (protected within 2 layers of 5/8-inch Type X gypsum board)

Table 26 Dimensions of EC-8.

Column	Grade (ksi)	Part	D (in.)	B (in.)	R (in.)	d (in.)	t (in.)
EC-8	55	W08SD099	8	3.78	0.25	1.050	0.099

Table 27 Unbraced length of EC-8.

Column	Unbraced length	
	Major axis, x (ft.)	Minor axis, y (ft.)
EC-8	21.5	7.5

D.2. Applied loading in the fire situation

Table 28 Forces in column EC-8 in the fire situation.

Column	Axial force (k)	Shear force (k)	Moment (ft-k)
EC-8	2.26	0	0

D.3. Performance objective

The cold-formed steel column is required to maintain its load-bearing function during 1 hour of standard fire exposure on 4 sides.

D.4. Thermal analysis

The heat transfer analysis is carried out by finite element simulation. The software SAFIR is used. The thermal properties for steel are taken from the proposed AISI Fire Appendix. The thermal properties for gypsum board are taken from Cooper [12]. The emissivity is taken as 0.7 and the convection heat transfer coefficient is 25 W/m^2k (4.4 $Btu/(hr \cdot ft^2 \cdot °F)$).

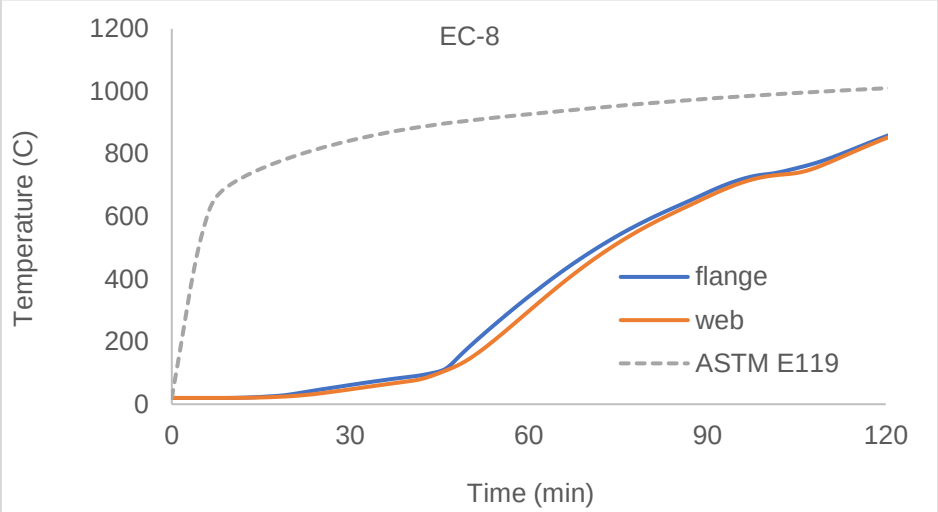

Figure 39 Temperature history at the flange and web of EC-8.

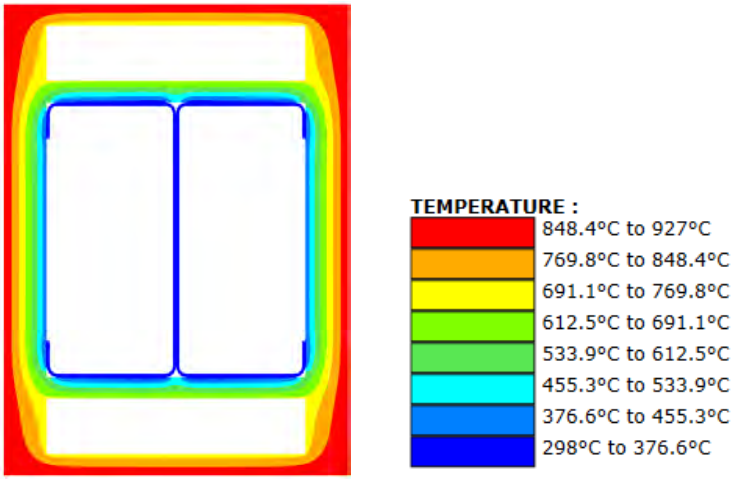

Figure 40 Temperature distribution at 60 minutes under ASTM E119 fire.

D.5. Nominal Strength at ambient temperature

D.5.1. AISI S100 DSM

(16) Global buckling strength

Cross-section properties

The cross-section properties are calculated from the open-source program CUFSM [23].

$A = 1.67\ in^2$	$I_x = 17.1\ in^4$	$I_y = 3.30\ in^4$
$J = 0.00544\ in^4$	$C_w = 44.5\ in^6$	$x_0 = -2.99\ in$
$r_x = 3.21\ in$	$r_y = 1.41\ in$	$r_0 = 4.60\ in$

Length and bracing conditions

$K_x = 1$	$K_y = 1$	$K_t = 1$
$L_x = 90\ in$	$L_y = 258\ in$	$L_t = 90\ in$

Retention factors (ambient)

$T = 68\ °\text{F}$	$k_E = 1.00$	$k_y = 1.00$
$E = 29500\ ksi$	$F_y = 55\ ksi$	$G = 11346\ ks$

Individual buckling modes

$\sigma_{ex} = 44.9\ ksi$	$\sigma_{ey} = 71.0\ ksi$	$\sigma_t = 47.0\ ksi$

Torsional-flexural buckling

$F_{cre} = 27.8\ ksi$

$$\lambda_c = \sqrt{\frac{F_y}{F_{cre}}} = 1.41 < 1.5$$

$F_n = 0.658^{\lambda_c^2} F_y = 24.1\ ksi$

The global buckling strength is: $P_{ne} = AF_n = 40.1\ kip$

(17) Local buckling strength

Web local buckling

$k = 4$	$t = 0.099\ in$	$w = 7.40\ in$
$F_{crl\_web} = 19.1\ ksi$		

Flange local buckling

$k = 4$ $t = 0.099\ in$ $w = 3.18\ in$
$F_{crl\_flange} = 103\ ksi$

Lip local buckling

$k = 0.43$ $t = 0.099\ in$ $w = 0.751\ in$
$F_{crl\_lip} = 199\ ksi$

$F_{crl} = \min(F_{crl_{web}} \quad F_{crl_{flange}} \quad F_{crl_{lip}}) = 19.1\ ksi$

$P_{crl} = AF_{crl} = 31.8\ kip$

$$\lambda_l = \sqrt{\frac{P_{ne}}{P_{crl}}} = 1.12 > 0.776$$

$$P_{nl} = \left[1 - 0.15\left(\frac{P_{crl}}{P_{ne}}\right)^{0.4}\right]\left(\frac{P_{crl}}{P_{ne}}\right)^{0.4} P_{ne} = 31.5\ kip$$

(18) Distortional buckling strength

Mid-line dimensions of cross-section

$b = 3.68\ in$ $d = 1.00\ in$ $h = 7.90\ in$
$t = 0.0990\ in$ $h_o = 8.00\ in$

Cross-section properties

The cross-section properties are calculated from the open-source program CUFSM [23].

$A_f = 0.463\ in^2$ $J_f = 0.00151\ in^4$ $I_{xf} = 0.0280\ in^4$
$I_{yf} = 0.675\ in^4$ $I_{xyf} = 0.0717\ in^4$ $C_{wf} = 0.00\ in^2$
$x_{of} = 1.45\ in$ $y_{of} = -0.107\ in$ $h_{xf} = -2.23\ in$
$h_{yf} = -0.107\ in$

F_{crd}

$L_{crd} = 33.2\ in$ $L_m = 33.2\ in$ $L = 33.2\ in$
$k_{\phi fe} = 0.809\ kip$ $k_{\phi we} = 0.655\ kip$ $k_{\phi fg} = 0.0280\ in^2$
$k_{\phi wg} = 0.00757\ in^2$ $k_\phi = 0$ $F_{crd} = 41.1\ ksi$

$$P_{crd} = AF_{crd} = 68.5\ kip$$

$$\lambda_d = \sqrt{\frac{P_y}{P_{crd}}} = 1.16 > 0.561$$

$$P_y = AF_y = 91.6\ kip$$

$$P_{nd} = \left[1 - 0.25\left(\frac{P_{crd}}{P_y}\right)^{0.6}\right]\left(\frac{P_{crd}}{P_y}\right)^{0.6} P_y = 60.8\ kip$$

(19) Nominal capacity at ambient temperature

$\lambda_c = 1.41$ $P_{ne} = 40.1\ kip$

$\lambda_l = 1.12$ $P_{nl} = 31.5\ kip$

$\lambda_d = 1.16$ $P_{nd} = 60.8\ kip$

$$P_{DSM} = \min(P_{ne}, P_{nl}, P_{nd}) = P_{nl} = 31.5\ kip$$

The controlling failure mode is local buckling.

D.5.2. FEM analysis

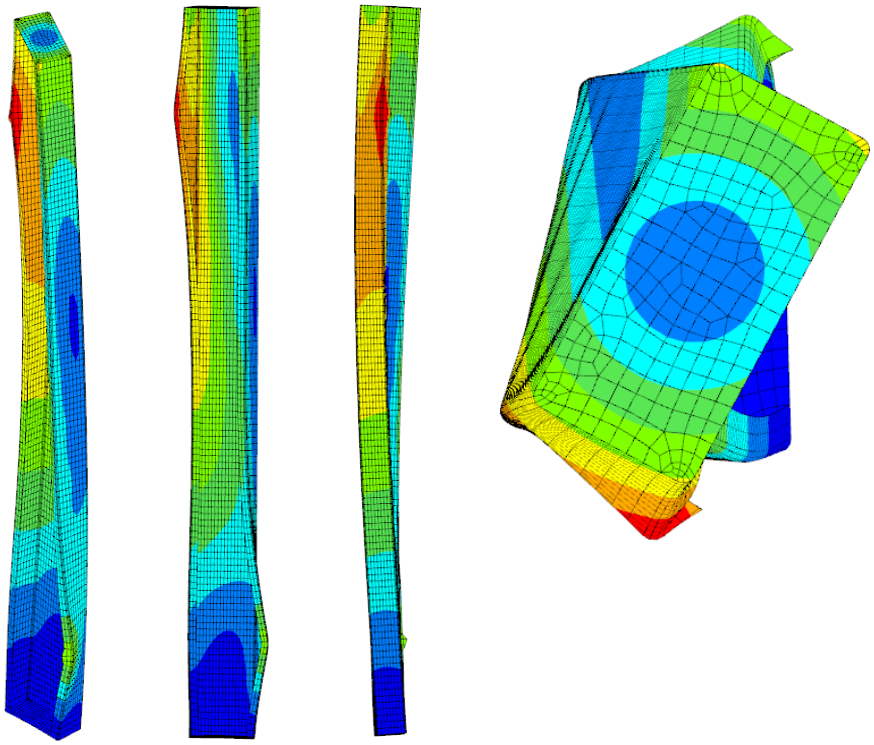

Figure 41 Failure mode at ambient temperature.

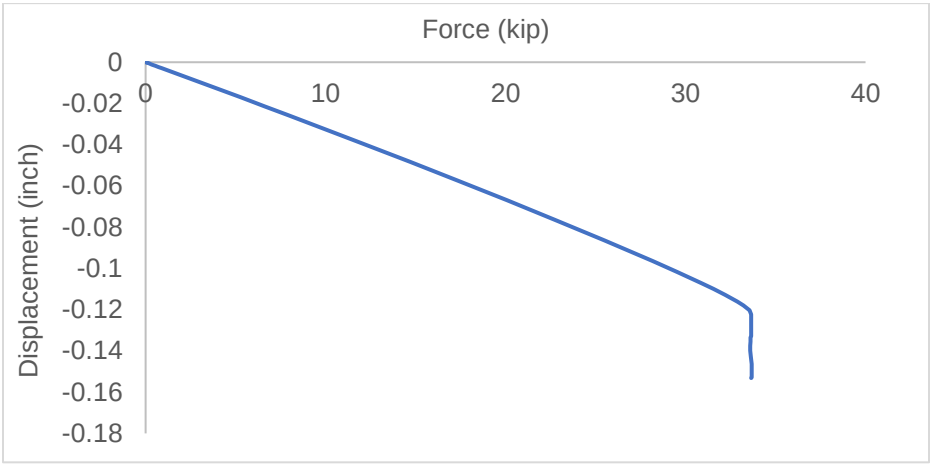

Figure 42 Force-displacement curve at ambient temperature.

Table 29 Capacity of column EC-8 at ambient temperature.

Columns	AISI S100 DSM Nominal Strength (kip)	SAFIR/Shell FE (kip)
EC-8	31.5	33.7

D.6. Nominal Strength at 60 minutes under ASTM E119 fire (AISI S100 DSM)

At 60 minutes, the steel temperature of EC-8 is 651 °F (344 °C). The reduction factors are taken at a temperature of 651 °F (344 °C).

(20) Global buckling strength

Retention factors

$T = 651$ °F	$k_E = 0.758$	$k_y = 0.804$
$E, T = 22355\ ksi$	$F_y, T = 44.2\ ksi$	$G, T = 8598\ ksi$

Individual buckling modes

$\sigma_{ex} = 34.0\ ksi$	$\sigma_{ey} = 53.8\ ksi$	$\sigma_t = 35.6\ ksi$

Torsional-flexural buckling

$F_{cre} = 21.1\ ksi$

$$\lambda_c = \sqrt{\frac{F_{y,T}}{F_{cre}}} = 1.45 < 1.5$$

$F_n = 0.658^{\lambda_c^2} F_{y,T} = 18.4\ ksi$

The global buckling strength is: $P_{ne} = AF_n = 30.6\ kip$

(21) Local buckling strength

Web local buckling

$k = 4$	$t = 0.099\ in$	$w = 7.40\ in$
$F_{crl\_web} = 14.4\ ksi$		

Flange local buckling

$k = 4$	$t = 0.099\ in$	$w = 3.18\ in$
$F_{crl\_flange} = 78.2\ ksi$		

Lip local buckling

$k = 0.43$	$t = 0.099\ in$	$w = 0.751\ in$
$F_{crl\_lip} = 151\ ksi$		

$F_{crl} = \min (F_{crl_{web}} \quad F_{crl_{flange}} \quad F_{crl_{lip}}) = 14.4\ ksi$

$P_{crl} = AF_{crl} = 24.1\ kip$

$$\lambda_l = \sqrt{\frac{P_{ne}}{P_{crl}}} = 1.13 > 0.776$$

$$P_{nl} = \left[1 - 0.15\left(\frac{P_{crl}}{P_{ne}}\right)^{0.4}\right]\left(\frac{P_{crl}}{P_{ne}}\right)^{0.4} P_{ne} = 24.0\ kip$$

(22) Distortional buckling strength

$\boldsymbol{F_{crd}}$

$L_{crd} = 33.2\ in$	$L_m = 33.2\ in$	$L = 33.2\ in$
$k_{\phi fe} = 0.613\ kip$	$k_{\phi we} = 0.497\ kip$	$k_{\phi fg} = 0.0280\ in^2$
$k_{\phi wg} = 0.00757\ in^2$	$k_\phi = 0$	$F_{crd} = 31.2\ ksi$

$$P_{crd} = AF_{crd} = 51.9\ kip$$

$$\lambda_d = \sqrt{\frac{P_y}{P_{crd}}} = 1.19 > 0.561$$

$$P_y = AF_{y,T} = 73.6\ kip$$

$$P_{nd} = \left[1 - 0.25\left(\frac{P_{crd}}{P_y}\right)^{0.6}\right]\left(\frac{P_{crd}}{P_y}\right)^{0.6} P_y = 47.6\ kip$$

(23) Nominal capacity at 60 minutes under ASTM E119 fire

$\lambda_c = 1.45$	$P_{ne} = 30.6\ kip$
$\lambda_l = 1.13$	$P_{nl} = 24.0\ kip$
$\lambda_d = 1.19$	$P_{nd} = 47.6\ kip$

$$P_{DSM} = \min(P_{ne}, P_{nl}, P_{nd}) = P_{ne} = 24.0\ kip$$

The controlling failure mode is local buckling.

D.7. Failure temperature and failure time

D.7.1. AISI S100 DSM

After the iteration, the failure temperature is 904 °C (1,659 °F).

(24) Global buckling strength

Retention factors

$T = 1659$ °F $\quad k_E = 0.0772 \quad k_y = 0.0530$

$E, T = 2276\ ksi \quad F_y, T = 2.92\ ksi \quad G, T = 876\ ksi$

Individual buckling modes

$\sigma_{ex} = 3.47\ ksi \quad \sigma_{ey} = 5.48\ ksi \quad \sigma_t = 5.48\ ksi$

Torsional-flexural buckling

$F_{cre} = 2.15\ ksi$

$$\lambda_c = \sqrt{\frac{F_{y,T}}{F_{cre}}} = 1.16 < 1.5$$

$F_n = 0.658^{\lambda_c^2} F_{y,T} = 1.65\ ksi$

The global buckling strength is: $P_{ne} = AF_n = 2.75\ kip$

(25) Local buckling strength

Web local buckling

$k = 4 \quad t = 0.099\ in \quad w = 7.40\ in$

$F_{crl\_web} = 1.47\ ksi$

Flange local buckling

$k = 4 \quad t = 0.099\ in \quad w = 3.18\ in$

$F_{crl\_flange} = 7.96\ ksi$

Lip local buckling

$k = 0.43 \quad t = 0.099\ in \quad w = 0.751\ in$

$F_{crl\_lip} = 15.4\ ksi$

$F_{crl} = \min(F_{crl_{web}} \quad F_{crl_{flange}} \quad F_{crl_{lip}}) = 1.47\ ksi$

$P_{crl} = AF_{crl} = 2.45\ kip$

$\lambda_l = \sqrt{\frac{P_{ne}}{P_{crl}}} = 1.06 > 0.776$

$P_{nl} = \left[1 - 0.15\left(\frac{P_{crl}}{P_{ne}}\right)^{0.4}\right]\left(\frac{P_{crl}}{P_{ne}}\right)^{0.4} P_{ne} = 2.25\ kip$

(26) Distortional buckling strength

$\boldsymbol{F_{crd}}$

$L_{crd} = 33.2\ in$ $L_m = 33.2\ in$ $L = 33.2\ in$

$k_{\phi fe} = 0.0624\ kip$ $k_{\phi we} = 0.0506\ kip$ $k_{\phi fg} = 0.0280\ in^2$

$k_{\phi wg} = 0.00757\ in^2$ $k_{\phi} = 0$ $F_{crd} = 3.17\ ksi$

$P_{crd} = AF_{crd} = 5.29\ kip$

$\lambda_d = \sqrt{\frac{P_y}{P_{crd}}} = 0.959 > 0.561$

$P_y = AF_{y,T} = 4.86\ kip$

$P_{nd} = \left[1 - 0.25\left(\frac{P_{crd}}{P_y}\right)^{0.6}\right]\left(\frac{P_{crd}}{P_y}\right)^{0.6} P_y = 3.77\ kip$

(27) Nominal capacity at temperature of 904 °C (1659 °F)

$\lambda_c = 1.16$ $P_{ne} = 2.75\ kip$

$\lambda_l = 1.06$ $P_{nl} = 2.25\ kip$

$\lambda_d = 0.959$ $P_{nd} = 3.77\ kip$

$P_{DSM} = \min(P_{ne}, P_{nl}, P_{nd}) = P_{ne} = 2.25\ kip$

The controlling failure mode is local buckling.

$P_{DSM} = 2.25\ kip \approx F = 2.26\ kip$

Utilization ratio$= \frac{P_{DSM}}{F} \approx 1.00$

From thermal analysis: $T_f = 904℃\ @\ t = 127\ min$

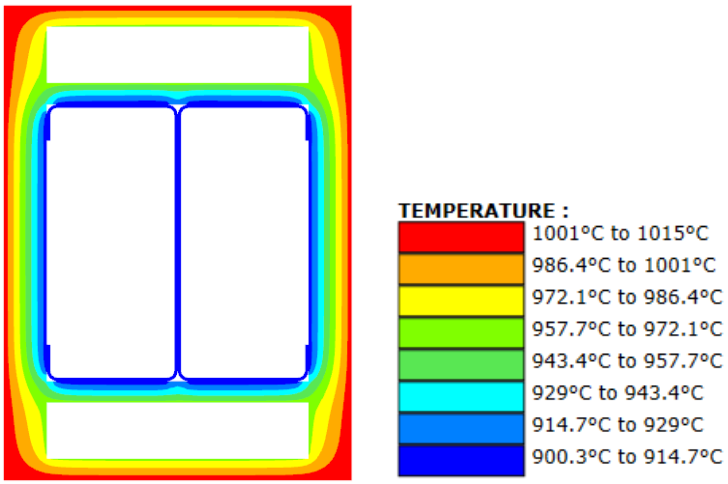

Figure 43 Temperature distribution at 127 minutes under ASTM E119 fire.

D.7.2. FEM analysis

A transient analysis is run until failure. Failure occurs after 127 minutes of fire exposure. From the thermal analysis, the member temperature is 900 °C (1,652 °F) at the time of failure.

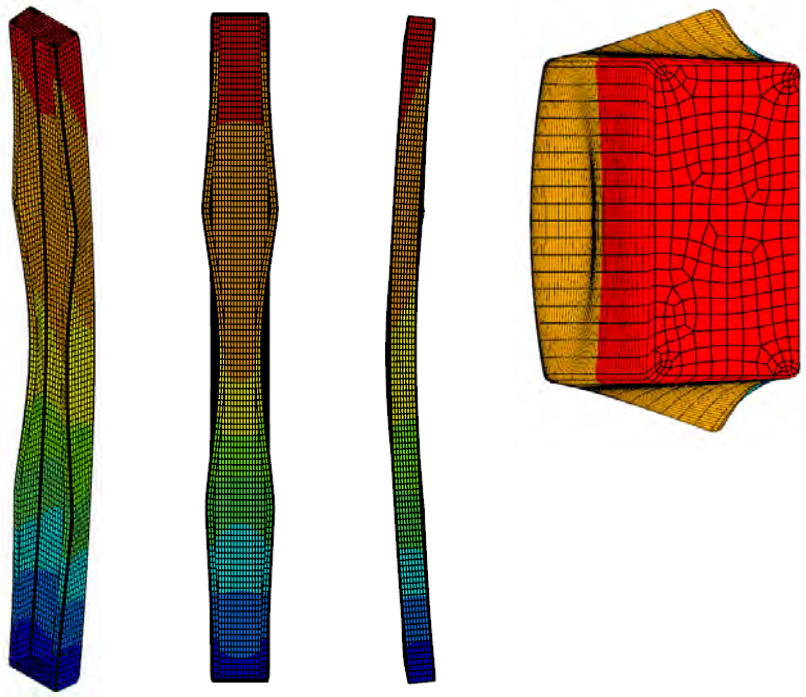

Figure 44 Failure mode under ASTM E119 fire.

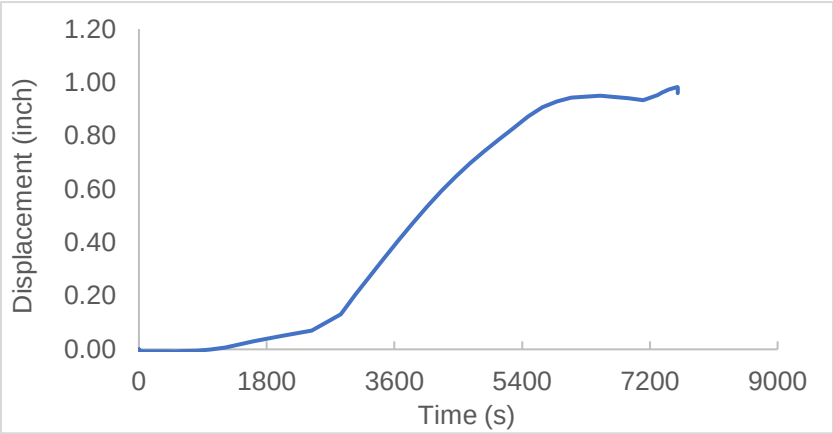

Figure 45 Vertical displacement at the loading end under ASTM E119.

Table 30 Failure time and failure temperature under ASTM E119.

Columns	DSM		SAFIR/Shell FE	
	Failure time (min)	Failure temperature (°F/°C)	Failure time (min)	Failure temperature (°F/°C)
EC-8	127	1659 / 904	127	1652 / 900

Appendix E. Fire resistance rating of column assemblies based on limiting temperature (ASTM E119)

Note: thermal analyses in this appendix are conducted using the thermal properties of gypsum board from Cooper [12], as provided in Figure 14. Type X gypsum boards are assumed in these assemblies.

E.1. Assembly EC-6 temperatures

Thickness of gypsum (Type X)	1 x 1''	2 x ½''	2 x 5/8''	3 x 5/8''	2 x 1''
Configuration	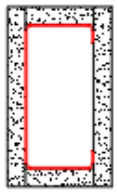	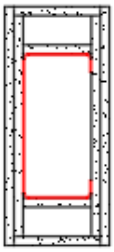	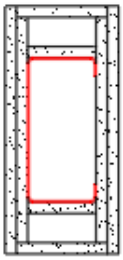	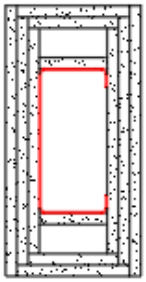	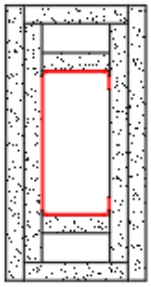
Temperature @1 hr.	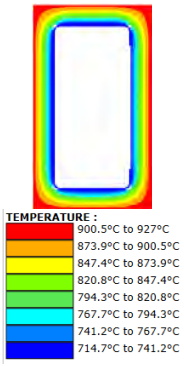	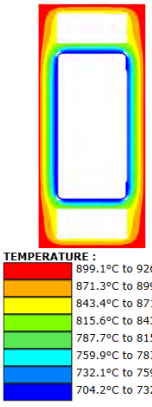	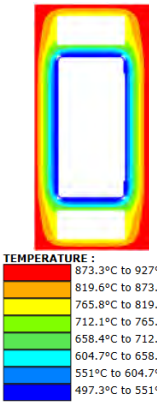	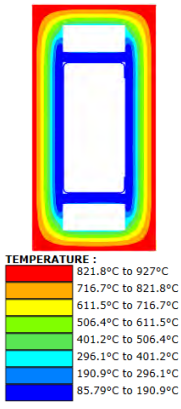	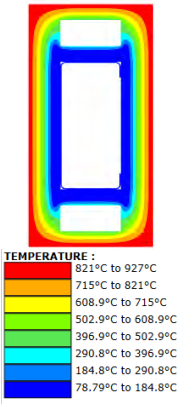
	$T_f = 715°C$ $T_w = 715°C$ $T_{avg} = 716°C$	$T_f = 706°C$ $T_w = 704°C$ $T_{avg} = 705°C$	$T_f = 499°C$ $T_w = 498°C$ $T_{avg} = 499°C$	$T_f = 86°C$ $T_w = 88°C$ $T_{avg} = 87°C$	$T_f = 79°C$ $T_w = 81°C$ $T_{avg} = 81°C$
Temperature @2 hr.	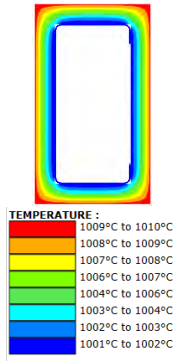	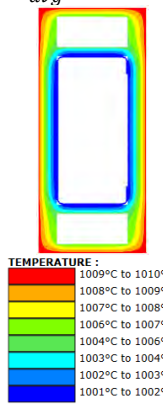	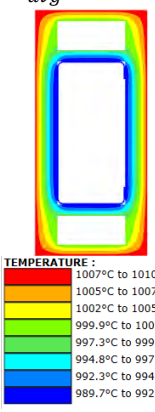	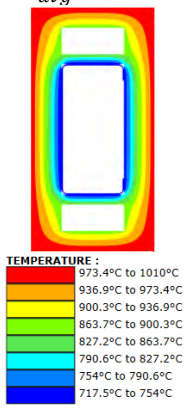	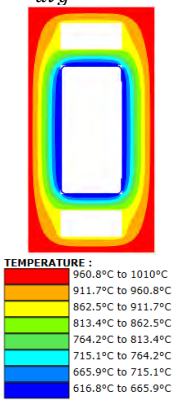
	$T_f = 1001°C$ $T_w = 1001°C$ $T_{avg} = 1001°C$	$T_f = 1001°C$ $T_w = 1001°C$ $T_{avg} = 1001°C$	$T_f = 990°C$ $T_w = 990°C$ $T_{avg} = 990°C$	$T_f = 721°C$ $T_w = 718°C$ $T_{avg} = 718°C$	$T_f = 612°C$ $T_w = 617°C$ $T_{avg} = 621°C$

Thickness of gypsum (Type X)	1 x 1''	2 x ½''	2 x 5/8''	3 x 5/8''	2 x 1''
Configuration	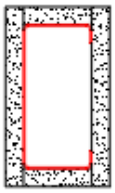	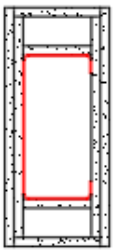	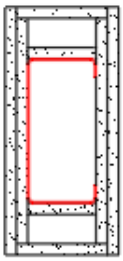	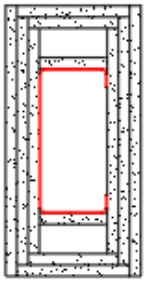	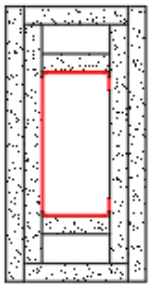
Temperature @1 hr.	$T_f = 1319°F$ $T_w = 1319°F$ $T_{avg} = 1321°F$	$T_f = 1303°F$ $T_w = 1299°F$ $T_{avg} = 1301°F$	$T_f = 930\,°F$ $T_w = 928\,°F$ $T_{avg} = 930\,°F$	$T_f = 187\,°F$ $T_w = 190\,°F$ $T_{avg} = 189\,°F$	$T_f = 174\,°F$ $T_w = 178\,°F$ $T_{avg} = 178\,°F$
Temperature @2 hr.	$T_f = 1834°F$ $T_w = 1834°F$ $T_{avg} = 1834°F$	$T_f = 1834°F$ $T_w = 1834°F$ $T_{avg} = 1834°F$	$T_f = 1814°F$ $T_w = 1814°F$ $T_{avg} = 1814°F$	$T_f = 1330°F$ $T_w = 1324°F$ $T_{avg} = 1324°F$	$T_f = 1134°F$ $T_w = 1143°F$ $T_{avg} = 1150°F$

Thickness of gypsum (Type X)	1 x 1''	2 x ½''	2 x 5/8''	3 x 5/8''	2 x 1''
Configuration	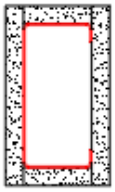	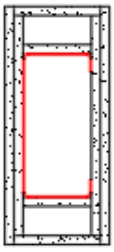	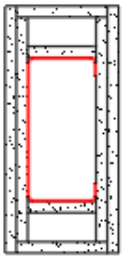	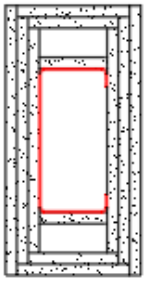	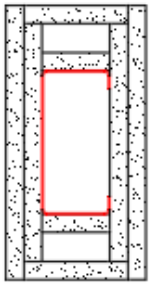
Fire resistance rating	-	-	1 hour	1 hour	1 hour

E.2. Assembly EC-8 temperatures

Thickness of gypsum (Type X)	1 x 1''	2 x ½''	2 x 5/8''	3 x 5/8''	2 x 1''
Configuration	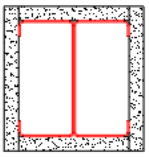	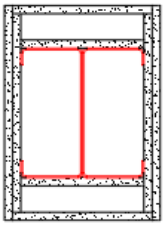	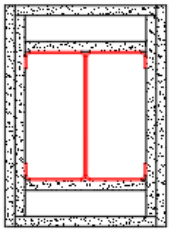	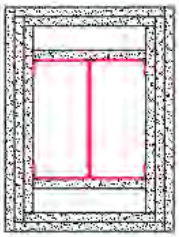	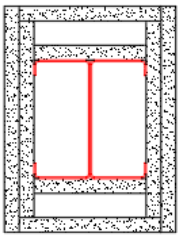
Temperature @1 hr.	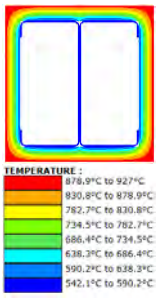 $T_f = 564°C$ $T_w = 543°C$ $T_{avg} = 556°C$	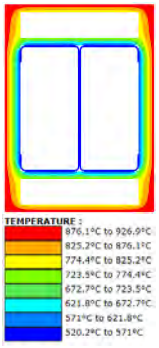 $T_f = 546°C$ $T_w = 520°C$ $T_{avg} = 535°C$	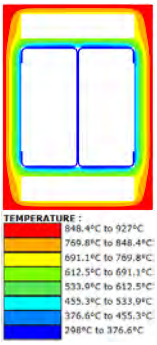 $T_f = 343°C$ $T_w = 298°C$ $T_{avg} = 344°C$	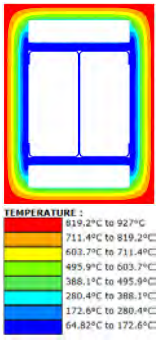 $T_f = 74°C$ $T_w = 65°C$ $T_{avg} = 70°C$	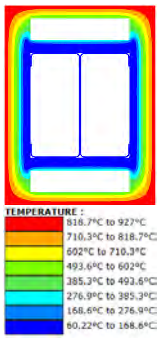 $T_f = 68°C$ $T_w = 60°C$ $T_{avg} = 71°C$
Temperature @2 hr.	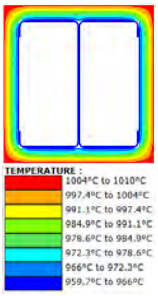 $T_f = 962°C$ $T_w = 960°C$ $T_{avg} = 960°C$	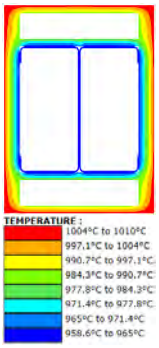 $T_f = 961°C$ $T_w = 959°C$ $T_{avg} = 960°C$	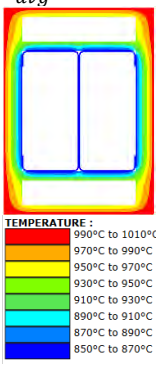 $T_f = 857°C$ $T_w = 850°C$ $T_{avg} = 857°C$	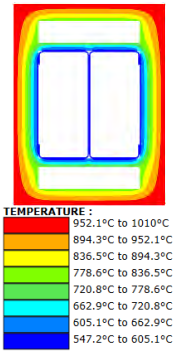 $T_f = 567°C$ $T_w = 547°C$ $T_{avg} = 558°C$	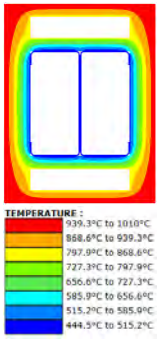 $T_f = 470°C$ $T_w = 444°C$ $T_{avg} = 476°C$

Thickness of gypsum (Type X)	1 x 1''	2 x ½''	2 x 5/8''	3 x 5/8''	2 x 1''
Configuration	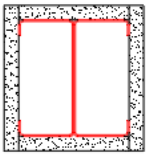	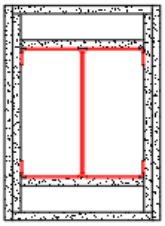	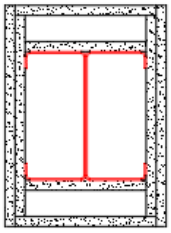	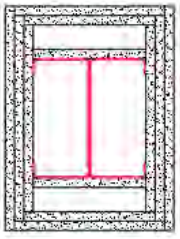	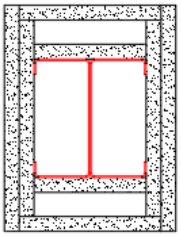
Temperature @1 hr.	$T_f = 1047°F$ $T_w = 1009°F$ $T_{avg} = 1033°F$	$T_f = 1015°F$ $T_w = 968°F$ $T_{avg} = 995°F$	$T_f = 649°F$ $T_w = 568°F$ $T_{avg} = 651°F$	$T_f = 165°F$ $T_w = 149°F$ $T_{avg} = 159°F$	$T_f = 154°F$ $T_w = 140°F$ $T_{avg} = 160°F$
Temperature @2 hr.	$T_f = 1764°F$ $T_w = 1760°F$ $T_{avg} = 1760°F$	$T_f = 1762°F$ $T_w = 1759°F$ $T_{avg} = 1760°F$	$T_f = 1575°F$ $T_w = 1562°F$ $T_{avg} = 1575°F$	$T_f = 1053°F$ $T_w = 1017°F$ $T_{avg} = 1036°F$	$T_f = 878°F$ $T_w = 831°F$ $T_{avg} = 889°F$

Thickness of gypsum (Type X)	1 x 1''	2 x ½''	2 x 5/8''	3 x 5/8''	2 x 1''
Configuration	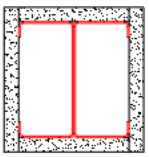	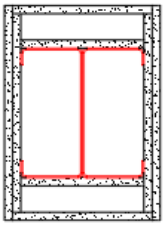	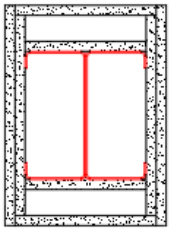	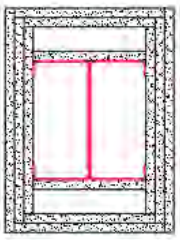	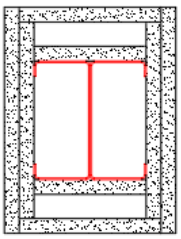
Fire resistance rating	-	1 hour	1 hour	1 hour	2 hours

Appendix F. Thermal properties of gypsum board collected from literature

Note: the tabulated values provided hereafter have been estimated from curves published by different authors. The reader is referred to the publications listed in the references for the original data.

F.1. Thermal conductivity

Cooper		Mehaffey		Manzello		Andersson	
T (°C)	k (W/(mK))	T (°C)	k (W/(mK))	T (°C)	k (W/(mK))	T (°C)	k (W/(mK))
0	0.225	0	0.225	20	0.140	0	0.273
75	0.225	75	0.202	50	0.159	58	0.257
90	0.225	90	0.185	75	0.169	95	0.197
110	0.108	110	0.162	102	0.169	150	0.136
123	0.108	123	0.147	154	0.175	200	0.120
135	0.108	135	0.120	200	0.178	247	0.127
146	0.108	146	0.120	249	0.183	300	0.136
370	0.108	370	0.115	305	0.188	352	0.162
605	0.164	605	0.126	351	0.193	401	0.178
672	0.183	672	0.137	400	0.199	451	0.210
687	0.187	687	0.140	452	0.206	502	0.240
800	0.243	800	0.146	502	0.210	551	0.271
1000	0.473	1000	0.230	548	0.214	603	0.310
		1200	0.314	600	0.228	652	0.349
				646	0.246	702	0.398
				698	0.257	753	0.462
						803	0.511

Thomas		Harmathy		Sultan	
T (°C)	k (W/(mK))	T (°C)	k (W/(mK))	T (°C)	k (W/(mK))
0	0.247	25	0.224	0	0.271
70	0.250	70	0.238	92	0.271
135	0.129	103	0.208	101	0.153
273	0.129	170	0.136	190	0.150
383	0.136	215	0.116	200	0.166
508	0.146	284	0.106	296	0.171
612	0.160	401	0.127	488	0.169
715	0.169	519	0.116	502	0.250
794	0.176	764	0.102	689	0.250
998	0.342			698	0.446
1000	0.775			1200	0.449

Cooper		Mehaffey		Manzello		Andersson	
T (°F)	k (Btu/(hr.ft.F))	T (°F)	k (Btu/(hr.ft.F))	T (°F)	k (Btu/(hr.ft.F))	T (°F)	k (Btu/(hr.ft.F))
32	0.130	32	0.130	68	0.081	32	0.158
167	0.130	167	0.117	122	0.092	136	0.148
194	0.130	194	0.107	167	0.098	203	0.114
230	0.062	230	0.094	216	0.098	302	0.079
253	0.062	253	0.085	309	0.101	392	0.069
275	0.062	275	0.069	392	0.103	477	0.073
295	0.062	295	0.069	480	0.106	572	0.079
698	0.062	698	0.066	581	0.109	666	0.094
1121	0.095	1121	0.073	664	0.112	754	0.103
1242	0.106	1242	0.079	752	0.115	844	0.121
1269	0.108	1269	0.081	846	0.119	936	0.139
1472	0.140	1472	0.084	936	0.121	1024	0.157
1832	0.273	1832	0.133	1018	0.124	1117	0.179
		2192	0.181	1112	0.132	1206	0.202
				1195	0.142	1296	0.230
				1288	0.148	1387	0.267
						1477	0.295

Thomas		Harmathy		Sultan	
T (°F)	k (Btu/(hr.ft.F))	T (°F)	k (Btu/(hr.ft.F))	T (°F)	k (Btu/(hr.ft.F))
0	0.247	25	0.224	0	0.271
70	0.250	70	0.238	92	0.271
135	0.129	103	0.208	101	0.153
273	0.129	170	0.136	190	0.150
383	0.136	215	0.116	200	0.166
508	0.146	284	0.106	296	0.171
612	0.160	401	0.127	488	0.169
715	0.169	519	0.116	502	0.250
794	0.176	764	0.102	689	0.250
998	0.342			698	0.446
1000	0.775			1200	0.449

F.2. Specific heat

Cooper		Mehaffey 20C/min		Mehaffey 2C/min		Konig J.	
T (°C)	c (J/(kgK))	T (°C)	c (J/(kgK))	T (°C)	c (J/(kgK))	T (°C)	c (J/(kgK))
0	1500	0	950	0	950	0	1210
75	1840	88	1360	64	1050	95	1210
90	7015	115	5590	85	8080	105	48500
110	13915	141	14200	92	13500	115	1210
123	18400	157	5640	104	29100	600	1210
135	2060	169	1170	106	25900	1200	360
146	983	200	950	109	13700		
370	850			114	950		
605	710			200	950		
672	3080						
687	611						
800	623						
1000	645						

Sultan M.A.	
T (°C)	c (J/(kgK))
20	1500
78	1842
85	2892
97	5913
124	18713
139	2024
148	1061
373	715
430	714
571	572
609	642
662	2960
670	3000
685	820
1000	571

Cooper		Mehaffey 20C/min		Mehaffey 2C/min		Konig J.	
T (°F)	c (J/(kgK))	T (°F)	c (J/(kgK))	T (°F)	c (J/(kgK))	T (°F)	c (J/(kgK))
32	0.358	32	0.227	32	0.227	32	0.289
167	0.439	190	0.325	147	0.251	203	0.289
194	1.675	239	1.335	185	1.930	221	11.584
230	3.324	286	3.392	198	3.224	239	0.289
253	4.395	315	1.347	219	6.950	1112	0.289
275	0.492	336	0.279	223	6.186	2192	0.086
295	0.235	392	0.227	228	3.272		
698	0.203			237	0.227		
1121	0.170			392	0.227		
1242	0.736						
1269	0.146						
1472	0.149						
1832	0.154						

Sultan M.A.	
T (°F)	c (J/(kgK))
68	0.358
172	0.440
185	0.691
207	1.412
255	4.469
282	0.483
298	0.253
703	0.171
806	0.171
1060	0.137
1128	0.153
1224	0.707
1238	0.717
1265	0.196
1832	0.136

References

[1] AISI S100-16, North American Cold-Formed Steel Specification for the Design of Cold-Formed Steel Structural Members, Washington, DC, 2016.

[2] ASTM E119-18c, Standard test methods for fire tests of building construction and materials, West Conshohocken, PA, 2018.

[3] International Code Council. International Building Code, Brea, CA, 2018.

[4] ASCE/SEI 7-16, Minimum Design Loads for Buildings and Other Structures, ASCE/SEI 7, Structural Engineering Institute of ASCE, Reston, VA, 2013. https://doi.org/10.1061/9780784412916.

[5] J.-F. Cadorin, J.-M. Franssen, A tool to design steel elements submitted to compartment fires—OZone V2. Part 1: pre-and post-flashover compartment fire model, Fire Saf. J. 38 (2003) 395–427.

[6] C.E.N. (European C. for Standardization), Eurocode 1: Actions on structures—Part 1-2: General actions—Actions on structures exposed to fire, (2002).

[7] N.F.P. Association, NFPA 557 Standard for Determination of Fire Load for Use in Structural Fire Protection Design, Massachusetts: NFPA, 2012.

[8] BSI, BS 7974:2019 Application of fire safety engineering principles to the design of buildings, BSI, London, 2019.

[9] N. Elhami-Khorasani, J.G. Salado Castillo, T. Gernay, A digitized fuel load surveying methodology using machine vision, Fire Technol. 57 (2021) 207–232.

[10] N. Elhami-Khorasani, J.G.S. Castillo, E. Saula, T. Josephs, G. Nurlybekova, T. Gernay, Application of a digitized fuel load surveying methodology to office buildings, Fire Technol. 57 (2021) 101–122.

[11] J.-M. Franssen, T. Gernay, Modeling structures in fire with SAFIR®: Theoretical background and capabilities, J. Struct. Fire Eng. (2017).

[12] L.Y. Cooper, The Thermal Response of Gypsum-panel/steel-stud Wall Systems Exposed to Fire Environments: A Simulation for Use in Zone-type Fire Models, US Department of Commerce, Technology Administration, National Institute of Standards and Technology, 1997.

[13] B.W. Schafer, The direct strength method of cold-formed steel member design, J. Constr. Steel Res. 64 (2008) 766–778.

[14] UL File R74066-6, -7: Report on steel columns protected with gypsum wallboard, CLEVELAND OHIO, 1978.

[15] L. Andersson, B. Jansson, Analytical fire design with gypsum—a theoretical and experimental study, Inst. Fire Saf. Des. Lund, Sweden. (1987).

[16] T.Z. Harmathy, The SFPE handbook of fire protection engineering, Soc. Fire Prot. Eng. Fire Prot. Assoc. Bost. (1988).

[17] G. Thomas, Thermal properties of gypsum plasterboard at high temperatures, Fire Mater. 26 (2002) 37–45.

[18] M.A. Sultan, A model for predicting heat transfer through noninsulated unloaded steel-stud gypsum board wall assemblies exposed to fire, Fire Technol. 32 (1996) 239–259.

[19] J.R. Mehaffey, P. Cuerrier, G. Carisse, A model for predicting heat transfer through

gypsum-board/wood-stud walls exposed to fire, Fire Mater. 18 (1994) 297–305.

[20] M. Samuel L., P. Suel-Hyun, M. Tensei, D. P.Bentz, Measurement of Thermal Properties of Gypsum Board At Elevated Temperatures, Proc. Fifth Int. Conf. Struct. Fire. (2008) 656–665.

[21] X. Yan, J.C.B. Abreu, R.S. Glauz, B.W. Schafer, T. Gernay, Simple Three-Coefficient Equation for Temperature-Dependent Mechanical Properties of Cold-Formed Steels, J. Struct. Eng. 147 (2021) 4021035.

[22] P. Keerthan, M. Mahendran. Numerical studies of gypsum plasterboard panels under standard fire conditions. Fire Safety Journal 53 (2012) 105-119.

[23] B.W. Schafer, S. Ádány, Buckling analysis of cold-formed steel members using CUFSM: conventional and constrained finite strip methods, in: Eighteenth Int. Spec. Conf. Cold-Formed Steel Struct. Orlando, FL, Citeseer, 2006.

American Iron and Steel Institute

25 Massachusetts Avenue, NW
Suite 800
Washington, DC 20001

www.steel.org

Research Report RP-22-02